UNIVERSITY OF CALIFORNIA, MERCED

Optimization and Comparison of Two Different Fiber Optical Parametric Oscillators for Coherent Raman Scattering Techniques

A Thesis submitted in partial satisfaction of the requirements for the degree of Master of Science

in

Biological Engineering and Small Scale Technologies (BEST) Graduate Program

by

Thompson Lu

Committee in charge:

Changqing Li, Chair
Anne Myers Kelley
Jennifer Lu

The Thesis of Thompson Lu is approved, and is acceptable in quality and form for publication on microfilm and electronically:

Dr. Jennifer Lu

Dr. Anne Myers Kelley

Dr. Changqing Li, Chair

University of California, Merced

2014

Acknowledgements

There are numerous people that I am indebted to for this milestone in my career. First, I would like to thank my research adviser Dr. Jay E. Sharping, who took on the challenge of teaching me the skills needed to work in an optics lab. I would not have made it this far without his invaluable guidance and support. Next, I would like to express my gratitude to my lab partner, mentor, and friend, Leily Kiani, in which her technical and emotional support greatly helped me during the difficult times of my study. I would also like to acknowledge my other lab mates Alessandro Castelli and Alison Huff for offering their feedback and support on my work. Outside of my lab, I would like to express my gratitude to my friends in the UC Merced Bobcat Band through their emotional support during times of stress in classes and research. Most importantly, I thank my family, especially my parents Hue Minh Chau and Thang Lu, who did everything in their power to support my ambition and goals.

Table of Contents

List of Tables and Figures

Abstract

Coherent Raman Scattering (CRS) microscopy is a technique used to image cells through the use of intrinsic chemical bonds, which allows for label free imaging at video rate speeds. Since the process is coherent the generated signal is orders of magnitude higher than spontaneous Raman microscopy. Many light sources have been developed for CRS microscopy, such as solid state optical parametric oscillators, supercontinuum sources, and fiber lasers. Fiber optical parametric oscillators (FOPOs) are tunable light sources based on the $\chi^{(3)}$ nonlinearity found in SiO_2. They have the potential to be integrated into compact and robust fiber components. This thesis describes an optimization for output power through tailoring the polarization at the output coupler and characterizes two FOPO systems for their applications in CRS microscopy. Chapter 1 gives a conceptual overview of spontaneous Raman, coherent anti-Stokes Raman scattering (CARS), stimulated Raman scattering (SRS) techniques as well as the pump sources typically used to perform CRS microscopy. Chapter 2 summarizes the physics for understanding FOPO operation. Chapter 3 describes our results for optimizing output power for a Nd:YVO_4 pumped FOPO by using a polarizing beam splitter with polarization dependent components. Chapter 4 illustrates a Ti:Sapphire pumped FOPO and compares its performance with the Nd:YVO_4 system.

Chapter 1

Coherent Raman Scattering Technique Principles

Introduction

In this chapter we discuss the basic theory behind spontaneous Raman scattering and coherent Raman scattering. We discuss the pump sources typically used for CRS and give a brief overview of fiber optical parametric oscillators (FOPOs). The advancements in tunable laser sources have pioneered the development of many different microscopy and imaging modalities. One opportunity these tunable light sources is for spectroscopy and imaging of biological samples with coherent Raman scattering (CRS) techniques such as coherent anti-Stokes Raman scattering (CARS) and stimulated Raman scattering (SRS), which have allowed for label free imaging with chemical sensitivity. Systems that are pumped by solid state optical parametric oscillators (OPO) and those based on Supercontinuum (SC) generation have generated much flexibility and allowed for many modes of obtaining information on biological samples. The current gold standard for CRS techniques is a synchronously pumped OPO emitting picosecond pulses [1]. The current drawback in using OPOs for imaging is due to the complexity of operation and sensitivity to environmental changes, which make it less appealing for clinical use. However, in order to have a large impact factor, we must design light sources that the non-laser physicist can use.

Raman Scattering

Raman scattering is a powerful phenomenon that has made significant impacts in science and engineering. When light interacts with molecules, the photons can either be absorbed or scattered. In the scattering process, photons typically maintain their momentum and energy: this is known as Rayleigh scattering, or elastic scattering. However, when the photons experience a change in momentum after scattering, this is known as Raman scattering, or inelastic scattering. Raman photons scattered with lower energy are considered as Stokes photons; the photons scattered with higher energy are called anti-Stokes photons [2]. The conditions for the Raman scattering can only occur when the difference between incident and scattered photon energies matches a vibrational energy of the material. This allows for correlating a specific chemical bond vibrational mode to an energy value, represented as a wavenumber. In typical Raman spectrographs, the intensity of scattered photons is plotted as a function of Raman shifts relative to the wavenumber of the pump source. The general method to perform Raman spectroscopy is to use a single laser source, and either excite each Raman mode point by point (narrowband) or to excite all the Raman modes at once and utilize a Fourier transform technique to recover the Raman shift information (broadband). There have been many documented Raman spectra for different materials and chemicals in the literature, and it serves as a powerful reference for identification of compounds [2].

The drawback of using Raman techniques is the low photon count that carries useful chemical information. Only one out of 10^6 to 10^8 photons are Raman scattered for non-resonant spontaneous Raman scattering [2]. In order to increase the detection rate, one requires high quality filters, highly sensitive detectors, and high powered pump sources, together with plasmonic substrates, long pump exposure times, or resonance

enhancement. While changing the detection scheme can improve signal to noise ratio, the most direct approach for obtaining more Raman scattered photons is to increase the light source intensity. However, increasing the intensity may cause sample damage and degrade the Raman signal quality.

Raman Imaging

One can obtain an image and associate each pixel with a Raman signal. This approach gives chemical information about the image. Most Raman imaging has been performed with scanning instrumentation, where the beam is scanned across the sample to generate Raman spectra. The spectra in each area of the sample can be then overlapped to map out an image with chemical information. The scanning approaches are most commonly used in commercial Raman microscopes. However, due to the low sensitivity and long image acquisition times for spontaneous Raman microscopes, nonlinear Raman imaging modalities are considered an alternative system [3].

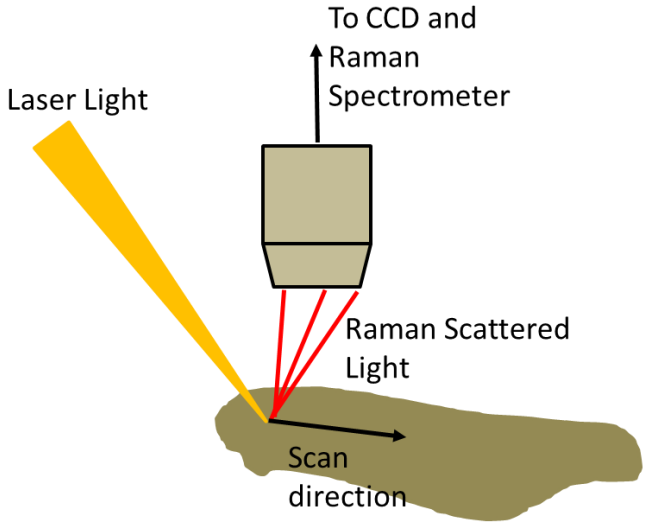

Fig 1.1 Schematic of a Raman microscope. The laser illuminates each point of the sample and objectives capture the Raman scattered light. An image of a point is taken with a CCD camera while a Raman spectrometer is used to obtain Raman information at that point. The laser can then be scanned across the sample to get Raman information at each point.

Coherent Raman Scattering

In coherent Raman scattering (CRS), the Raman scattered photons are amplified by means of coherence from a pump field. Typical experimental setups for CRS involve spatially and temporally overlapping two fields, called pump and Stokes, of different colors and sending them to a sample of interest. When the pump and Stokes frequency difference resonates with a Raman mode, the Raman signal is significantly enhanced [4]. The main difference between spontaneous Raman and coherent Raman techniques is that for the latter there is a requirement of two incident fields of different frequencies to

generate the coherence. CRS involves probing specific Raman vibrational modes which are driven coherently due to the oscillations of ω_{pump} and ω_{Stokes}. In spontaneous Raman scattering the sample is irradiated with a laser at a fixed wavelength and the measured intensity is correlated with the Raman shift with respect to the laser wavelength. In CRS, a tunable laser source is used to specifically excite Raman modes. There are two popular techniques to perform CRS: coherent anti-Stokes Raman scattering (CARS) and stimulated Raman scattering (SRS). Figure 1.2 gives an energy diagram of the two processes. Both processes occur simultaneously, but the detection schemes differ.

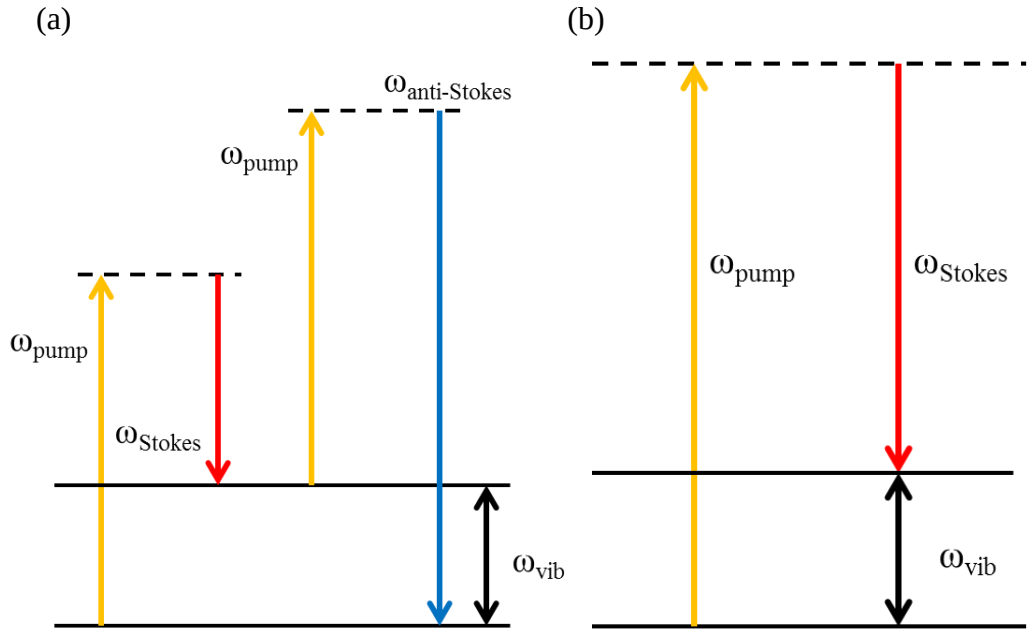

Figure 1.2 Energy diagrams of CARS and SRS. In CARS (a) the pump field excites a molecule to a virtual state. When ω_{pump} and ω_{Stokes} are resonant with a Raman vibrational mode, the molecule generates a coherence between the ground state and the excited vibrational state. The excited state can be probed by a second pump field, which generates a blueshifted signal at $\omega_{anti\text{-}Stokes}$ frequency. In SRS (b) the pump field excites the atom to a virtual state. When ω_{pump} and ω_{Stokes} are resonant with a Raman **v**ibrational mode, one pump photon is eliminated and one Stokes photon is created.

In CARS, the Raman signal is generated and detected at the anti-Stokes frequency. The technique is performed with pulsed lasers at different frequencies that correspond to a Raman vibration. The frequency generated in CARS is given as:

$$\omega_{anti\text{-}Stokes} = 2\omega_{pump} - \omega_{Stokes} \tag{1.1}$$

In a quantum mechanical picture, two pump photons are eliminated to produce a signal and an idler photon at different frequencies. The pump photon excites the material to a virtual state, in which then the material emits a Stokes photon through stimulated emission to reach an excited vibrational level of the ground state. Another pump photon

then excites the Stokes photon to a different virtual state and the return to ground state generates an anti-Stokes photon that is blue shifted away from the Stokes or pump. As a result, the output color can be easily detected since the blue-shifted photon can be differentiated from fluorescence. However, there is a nonresonant background associated with CARS [4]. Methods to suppress the nonresonant background include polarization sensitive detection, lock in detection, destructive interference of the nonresonant background, or using computational methods to subtract the nonresonant from the resonant signal [4].

In SRS, the Raman signal is generated and detected at the frequency of the pump or Stokes field. When the difference between the pump and Stokes frequency corresponds to a Raman vibration, a pump photon becomes annihilated while a Stokes photon is generated. The conditions for SRS are given in the following equation:

$$\Omega_{vib} = \omega_s - \omega_p \tag{1.2}$$

where ω_s and ω_p are the frequency of the Stokes and pump fields, respectively, and Ω_{vib} is the Raman vibration of interest [4]. In contrast to CARS, the method of detection for SRS is to detect an intensity change in either the Stokes (stimulated Raman gain) or the pump (stimulated Raman loss) field. Experimentally, this manifests as a decrease in intensity of the pump field and an increase in intensity of the Stokes field. In practice we measure the intensity loss in the pump field.

In order to detect the small intensity change between the two fields, a sensitive measurement technique called lock in detection is utilized. For most current SRS microscopy and spectroscopy schematics one modulates—introducing variations in the amplitude or phase of the waveform—the pump field and detects the intensity change in the Stokes field.

For use in imaging, the two lasers combine, enter into the imaging port of the microscope, pass through an objective and focus to a point on the sample. Imaging is possible in the forward direction or in the backward scattering direction. Prior to detection, spectral filters separate the pump from the signal of interest. One of the two beams is modulated at high frequency by an acousto-optical or electro-optical modulator. The modulation of one of the two beams allows detection of the SRS signal on the other beam via a lock in amplifier. The measured signals are linearly proportional to the concentration of the targeted molecule, allowing for quantitative measurements [4]. Unlike other coherent Raman scattering techniques, SRS is free from the nonresonant background [4] and delivers an improved signal to noise ratio.

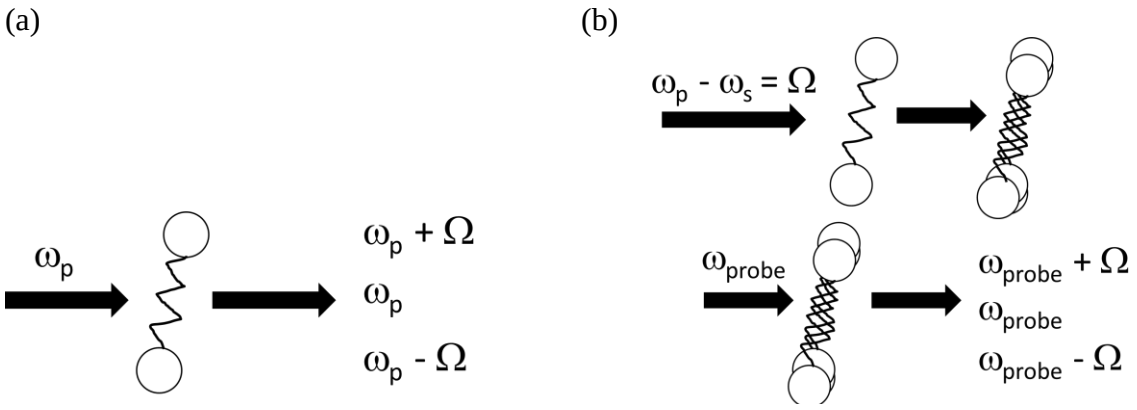

Figure 1.3 A ball and spring representation of spontaneous Raman scattering and CRS adapted from [4]. In spontaneous Raman scattering (a) the chemical bond is excited by an incident pump field at ω_p and the scattered components have frequencies at $\omega_p \pm$ the Raman vibration. In CRS (b), the difference between ω_p and ω_s matches a specific Raman mode and coherently drives the molecular vibrations. The excited state can then be probed by another field at ω_{probe}, which generates frequencies at $\omega_{probe} \pm$ Raman frequencies.

Raman Vibrational Modes

Both spontaneous Raman and CRS techniques probe the same Raman modes. However, the CRS technique generates a larger signal due to the coherent nature of excitation. For CARS, the nonresonant background introduces an extra step in data processing before it can be compared to the spontaneous Raman spectrum. On the other hand, SRS spectra can be directly compared to Raman spectra in the literature [4]. In order for a molecular vibration to be Raman active, that vibration must change the molecule's polarizability (the extent to which its electron cloud can be deformed by an electric field).

Chemical bonds can be modeled as masses on a spring. Hooke's law gives a relationship between the mass of the atoms and the frequency of vibration:

$$\nu = \frac{1}{2\pi c}\sqrt{\frac{K}{\mu}} \tag{1.3}$$

where ν is the frequency of oscillation, c is the speed of light, K is the force constant between the two masses, and μ is reduced mass of A and B, given as:

$$\mu = M_A M_B / (M_A + M_B) \tag{1.4}$$

Equations (1.3) and (1.4) indicate that as the masses of the two atoms get smaller, the frequency increases. Symmetric vibrations give the strongest Raman scattering [2]. Different atomic bonds give different vibrational resonances. In Raman spectra, the wavenumber range gives information regarding the chemical bonds. Hydrogen stretches appear in the 4000-2500 cm^{-1} region, multiple bond stretches in the 2500-2000 cm^{-1}

region, double bond stretches in the 2000-1500 cm^{-1} region, and below 1500 cm^{-1} is referred to as the fingerprint region [2].

For use in CRS microscopy and imaging one would prefer to select vibrations that are abundant in cells. Typically this has been the CH stretching modes found from around 2800 cm^{-1} to 3100 cm^{-1} [4]. Within the CH stretching modes minute differences between CH_2 and CH_3 stretching can be distinguished. This modality of imaging has found application for imaging cells with high lipid contents, such as in lipid metabolism or neurons. Proteins can also be imaged from CH stretching modes due to the different ratios of CH vibrations between lipids and amino acids [2]. Other Raman modes have been selected for use in imaging, such as the amide I (C=O and C=C) at around 1655 cm^{-1} for proteins and symmetric phosphodiester stretch and ring breathing at 783-790 cm^{-1} for nucleic [4]. High frequency (greater than 2500 cm^{-1} Raman) vibrations tend to have stronger intensities, but modes in the lower frequency regions give information regarding structure [2]. A table of Raman modes of interest for CRS microscopy and imaging is given in Table 1.4:

Wavenumber (cm^{-1})	Bond	Vibration	Applications
3250	OH	Stretch	Water
2950	CH_3	Stretch	Lipids, Protein
2885	CH_2	Asym Stretch	Lipids
2845	CH_2	Sym Stretch	Lipids
2100	C-D	Stretch	Lipids
1742	C=O	Stretch	Protein, Lipids
1660	C=C	Stretch	Lipids
1655	C=O and C=C	(C=O and C=C) Amide I	Protein
1550	N-H and C-N	(N-H bend and C-N stretch) Amide II	Protein
1452	C-H	Bend	Lipids
1440	CH_2	Scissor	Lipids
1240	C-N and N-H	(C-N stretch and N-H bend) Amide III	Protein
1099	PO_2^-	Sym Stretch	Nucleic Acids
783 - 790	PO_2^- and C-X	Sym phosphodiester stretch and ring breathing	Nucleic Acids

Table 1.4 List of Raman wavenumbers and the applications for imaging in CRS microscopy [4].

Pump Sources for CRS

The ideal source for CRS microscopy and spectroscopy should be compact and must produce multiple synchronous pulse trains having narrowband spectra (~1 nm) in the near infrared. The frequency difference between the pulse trains must be tunable to allow for label free imaging of cells with chemical sensitivity that can be compared to the large collection of Raman spectra in the literature. For biological applications one would be interested in probing Raman modes that are commonly found in organic compounds, which range from 1000 cm^{-1} to 3000 cm^{-1}. The source should ideally deliver output peak power on the order of 1 kW (100 mW average power, 1 picosecond pulse duration, 80

MHz repetition rate) in each pulse train. The pulse duration is defined as the length of the optical packet while the repetition rate is the time spacing between each pulse. Picosecond pulses have been experimentally determined to be ideal for performing CRS processes because in the spectral domain the width of a picosecond pulse is comparable to a Raman line width [4]. Shorter femtosecond pulses allow for the excitation of multiple nonlinear phenomena at once, but come at the cost of having a low signal to noise ratio, loss of spectral selectivity, and potential photo damage to the sample [4]. For compactness and stability, picosecond fiber based light sources are attractive for use in the clinical setting.

Reference [4] gives concise details about the history of pump sources for CRS microscopy. The first CRS microscopy system was devised by Duncan et al. in 1982, in which they used a pulsed dye laser system for CARS microscopy. The next generation of pump sources used two Ti:Sapphire mode-locked lasers that are electronically synchronized. This system had the advantage of wide tunability, but was sensitive to mechanical vibrations and mode-locking stability. The next generation used a Nd:YVO_4 laser light to pump an optical parametric oscillator and frequency doubled the other component. This had the benefit of automatic spatial and temporal overlap at the output, but required that each crystal be reoptimized for each wavelength. The current pump source that is commercially available is a 1064 nm laser in which it is frequency doubled to pump an OPO. A summary of significant pump sources is given in Table 1.5.

Year	Ref.	Pump Source	CRS Technique	Comments
2003	[11]	Ti:Sapphire femtosecond oscillator	CARS	Spectral phase of femtosecond pulse is tailored to generate the required fields for CARS
2003	[12]	Ti:Sapphire femtosecond oscillator coupled into PCF for SC generation	CARS	CARS signal was lock-in detected, generated fs pulses limits resolution
2010	[13]	Ti:Sapphire picosecond laser with time lens source	CARS and SRS	Use of time-lens to synchronize two pulsed sources
2011	[14]	Femtosecond fiber laser pumped FOPO	Multimodal CARS	Required the exchange of fibers to increase the tunability
2011	[15]	Nd:YVO laser pumping one OPO	CARS	Signal and Idler or Pump and signal combinations to generate Raman wavenumber
2011	[15]	Nd:YVO laser pumping two OPOs	CARS	Use of three colors for higher order wave mixing
2011	[8]	Nd:VVO4 picosecond laser and Ti:Sapphire femtosecond laser with a pulse shaper and spatial light modulator	SRS	Multiplex excitation by using pulse shaper to tailor broad pump spectrum to probe Raman vibration resonances
2011	[16]	Ti:Sapphire femtosecond oscillator coupled into PCF for SC generation	SRS	SC is used to generate Stokes field from 765 to 1000 nm, tuning occurs by changing the temporal delay between pump and Stokes pulses
2012	[9]	Yb-doped fiber laser and tunable CW diode laser coupled into PCF for FWM	CARS	Seeding FWM to reduce group velocity mismatch and generate narrow sidebands
2013	[17]	Tunable Yb-doped fiber seeding a divide pulse amplifier pumping a PCF based FOPO	CARS	Signal from FOPO are combined with pump, paper indicates that FOPO noise is lower than FOPA noise
2014	[1]	Er doped fiber split into two arms to generate pump and Stokes	SRS	Mostly fiber enclosed pump source, contains many amplifiers

Table 1.5 A list of pump sources used for CRS Techniques

Optical parametric oscillators are tunable light sources based on the $\chi^{(2)}$ susceptibility of nonlinear crystals. The operating principle for an OPO is described as a nonlinear process in which a pump photon propagating in a nonlinear optical crystal breaks down into two lower energy photons [6]. In order for the system to function energy and propagation equations must be satisfied:

$$\omega_p = \omega_s + \omega_i \quad (1.5)$$
$$\mathbf{k_p} = \mathbf{k_s} + \mathbf{k_i} \quad (1.6)$$

where ω corresponds to the frequencies of pump, signal, and idler and **k** corresponds to the propagation vector of pump, signal, and idler. These equations are analogous to the requirements needed to operate a FOPO. In a normal dispersive and isotropic medium, it is difficult to satisfy phase matching because the momentum of the pump photon is too large due to dispersion in the material, while in anisotropic materials, the momentum of the pump photon varies with the direction of propagation [6]. Changing orientation of the crystal is a basic way to tune an OPO. The bandwidth of the generated frequencies from the parametric process is determined by the length of the crystals [6].

Although tunable lasers are common in research and industrial settings, the wavelength coverage may be limited. For instance, the industry and research workhorse Ti:Sapphire laser system performs poorly at wavelengths greater than 1050 nm [7]. The purpose of an OPO is to increase the tunability range. Solid state OPOs can be complicated and cumbersome to use as one must pay attention to the temperature as well as the orientation of the nonlinear crystal orientation to maintain optimum operation.

In SC, a pump pulse is spectrally broadened as it goes through a material. The spectral broadening occurs due to a combination of many nonlinear phenomena occurring at the same time. Photonic crystal fibers (PCF) are commonly used to generate a SC spectrum. The SC spectrum can be tailored by spectral filtering and shaping to obtain the desired color for CRS [8]. The drawback of SC is the noise generated from contributions of many nonlinear processes occurring at once. This can lead to degradation in signal to noise ratios [9].

Fiber optical parametric oscillators are tunable laser sources based on the $\chi^{(3)}$ properties of SiO_2 optical fibers. Since the gain medium is a fiber, this type of system has potential to be completely fiber enclosed, addressing issues such as compactness and stability. In theory one could design a FOPO as a turn-key light source for performing nonlinear microscopy and spectroscopy. Not much work has been done with FOPOs for two main reasons: their solid state $\chi^{(2)}$ counter parts have been well studied and commercialized, and making an oscillator from optical fibers can prove difficult since there is more complexity in the physics in the fiber [10]. Figure 1.6 gives a general schematic for a multi pass FOPO in comparison to a single pass FOPA.

(a)

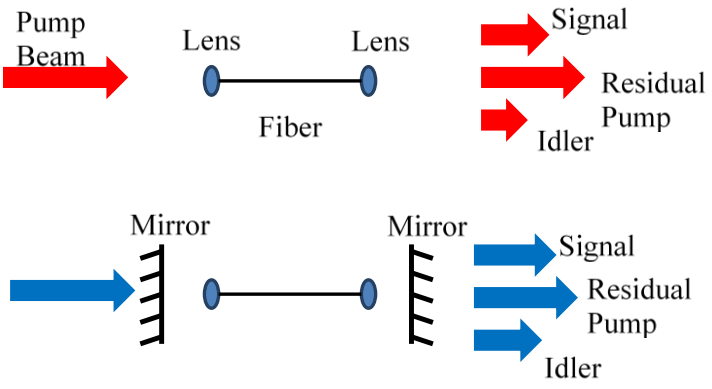

(b)

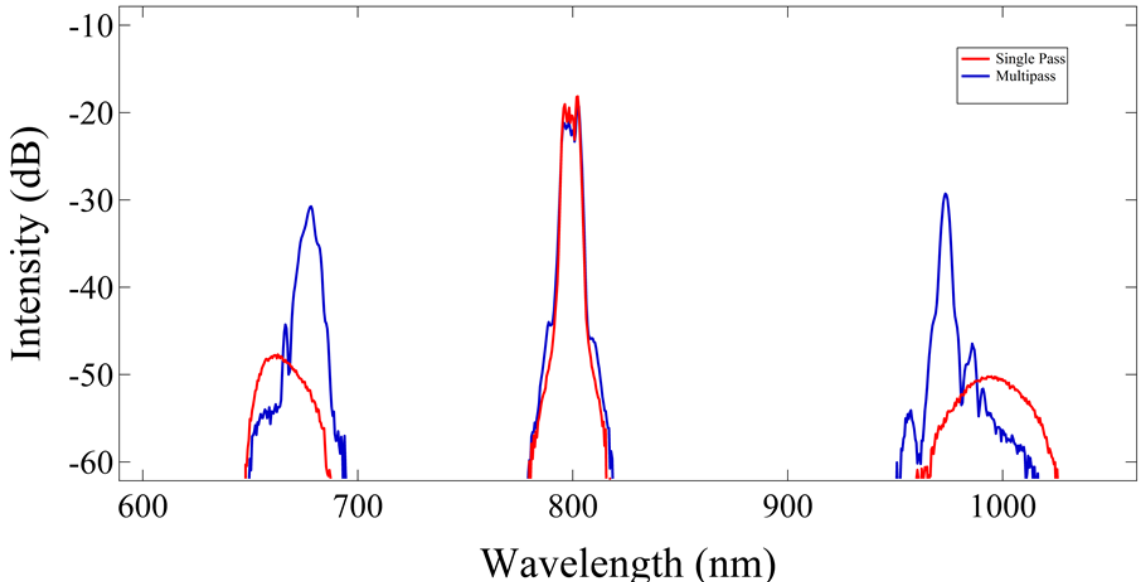

Figure 1.6 (a) A general schematic of the output for single pass (FOPA) and multi pass (FOPO) configurations for degenerate FWM. The single pass configuration is able to generate signal (blue) and idler (red) relative to the input pump. In the multi pass configuration the fiber is placed inside a semi-reflective cavity, which in turn allows for build-up of signal and idler fields.(b) A comparison of the outputs between a single pass and multi pass system.

We opted to use a Fabry-Perot cavity for our FOPOs, which allows for simple alignment and operation. However, there are two drawbacks in this set up. First, there are high losses within the cavity, but the problem can be mediated by increasing the reflectivity in the cavity. Second, there is some free space, in which the system is more susceptible to environmental issues than a fiber enclosed system. To overcome this issue, other arrangements can force the pump, signal, and idler to only propagate in one direction, such as in a ring cavity [10]. The drawback is that this set up is difficult to

assemble and we have less flexibility in optimizing the output power. For this thesis we opted to use a Fabry-Perot cavity setup for simple alignment.

With some optimizations we believe that FOPO based light sources can operate well enough for biomedical imaging and spectroscopy. They offer a relatively simplistic method of tuning, lower noise, and ease of operation in comparison to other similar types of systems. A distinct advantage of using FOPOs over their $\chi^{(2)}$ counterpart is that FOPOs can generate output wavelengths that are close to the pump which allows for matching Raman frequencies that are of biological interest [25]. However, FOPOs are still far away from being practical for CRS applications due to the lack of research in optimizing performance and the well advanced understanding in solid state systems.

FOPOs have been applied for CRS microscopy. Our group with collaboration with Cheng's group at Purdue University realized the first application of FOPOs to nonlinear microscopy. In their experiments, simultaneous CARS imaging of myelin sheath and two photon excitation fluorescence imaging of an axon in rat spinal cord was performed by utilizing a pulsed femtosecond fiber laser FOPO that covered a range of 840 to 930 nm [14]. The system had multiple drawbacks: fibers needed to be exchanged to increase the tunability, the bandwidth of the FOPO output was large compared to pump which limits the resolution, and the average output power could be improved upon. In the following years, [17] performed CARS imaging using a FOPO that is pumped by a tunable Yb-doped fiber laser operating in the picosecond regime. By using a tunable source their system had the flexibility to operate from 2710 to 3150 cm^{-1}, covering the entire range of high frequency CH_2 stretching modes, without the need to switch fibers with different dispersion characteristics. However, their system does not reach wavenumbers less than 1500 cm^{-1}, which are of interest for protein and nucleic acids.

Although FOPOs have come a long way in becoming practical for biological imaging and spectroscopy applications, there is still much work to be done. For this thesis we are interested in output coupling both sidebands with usable powers to increase the Raman modes that can be probed.

Chapter 2

FOPO Principles

Introduction

This chapter describes the physics behind FOPO operation. The chapter first gives a brief overview of polarization of light and how it is measured. Next, a short description of lasers and mode-locking is given. Then, the key points of nonlinear fiber optics such as photonic crystal fibers, pulse propagation, and equations that govern FWM are summarized. The chapter concludes with the comparisons of FOPOs to lasers and to another group of devices called FOPAs.

Polarization of Light

Light can be described as an electromagnetic wave oscillating in three dimensional space. The amplitude of the transverse wave can be decomposed into two sinusoidal components, x and y, that propagate in the z-direction. The phase difference between E_x and E_y determines the state of polarization of the light. A general expression for describing light propagation in free space is given as [18]:

$$E_x(z,t) = \hat{\imath}E_{0x}cos(kz - \omega t) \quad (2.1)$$
$$E_y(z,t) = \hat{\jmath}E_{0y}cos(kz - \omega t + \varepsilon) \quad (2.2)$$

Here E_0 is the amplitude, k is the propagation constant, z is the direction of propagation, ω is the frequency, and ε is the relative phase difference between the two oscillating waves. If ε is equal to 0 or multiples of π, then the wave is plane polarized since the two wave components are in phase with each other.

When looking head on at the oscillating field, the magnitude of E_x and E_y forms a trace. If ε is equal to odd multiples of $\pi/2$, then the wave is considered to be circularly polarized. The magnitude of E_x and E_y in this case draws out a circle. For ε equaling to anything other than multiples of π or $\pi/2$, then the state of polarization is considered elliptical. For the purposes of this experiment we restrict our analysis to plane polarized scenario.

Polarizers

A polarizer changes the input polarization state. Polarizers use four fundamental mechanisms: dichroism, reflection, scattering, and birefringence. There also must be asymmetry associated the mechanism. To determine if a device is a polarizer, one can utilize two polarizers and a detector. The relative orientation of the polarizers determines the intensity at the detector. This is known as Malus's Law, which is given as [18]:

$$I(\Theta) = I(0)cos^2\Theta \quad (2.3)$$

where I is irradiance, I(0) is the irradiance arriving at the second polarizer, and Θ is the angle between the transmission axes of the two polarizers [18]. The intensity can be correlated with the angle of the polarizer.

Waveplates

Waveplates are optics commonly employed to adjust polarization states. Waveplates are also known as retarders, because they change polarization states by retarding one of the components in the electromagnetic wave. They are typically birefringent materials that have different refractive indices commonly assigned to a fast axis and a slow axis. Different polarizations can be obtained by inducing a phase difference between the two components due to the birefringence of the waveplate.

There are two particularly useful waveplates. Half wave plates are designed so that the relative phases between the two components are delayed by π, while quarter waveplates have a phase delay of $\pi/2$. For this thesis we will use half wave plates which rotate the plane of polarization.

In using a half wave plate and another polarizing optic called a polarizing beam splitter (PBS), it is possible to estimate the degree of polarization of light. By rotating one of the polarizers, we can measure how well the light is transmitted through the polarizers, also known as visibility. One would measure the visibility of the light, which is given by:

$$V = \frac{P_{max} - P_{min}}{P_{max} + P_{min}} \tag{2.4}$$

where P_{max} is the maximum power detected, P_{min} is the minimum power detected, and V is the visibility. A schematic of how to measure visibility is given in Figure 2.1.

For our visibility measurements, we have two polarizing optics, a half wave plate (HWP) and a polarizing beam splitter (PBS). As we rotate HWP, the input polarization state is going to change. Going through the PBS separates horizontal and vertical states. The transmitted horizontal state is then measured on a power meter. When the input polarization is plane polarized, the difference between P_{max} and P_{min} will be large since the state of polarization can be oriented to be either completely transmitted or reflected. The power versus wave plate rotation plot is a sinusoidal curve, resulting in a visibility close to 1. However, when the input polarization state is circular or unpolarized, the separated components have equal horizontal and vertical characteristics, which manifests in no difference in to the reading in the detector. The power versus wave plate rotation plots is closer to a horizontal line, resulting in a visibility of close to 0. We will use the visibility calculation to determine the state of the polarization for the polarization based output coupling scheme.

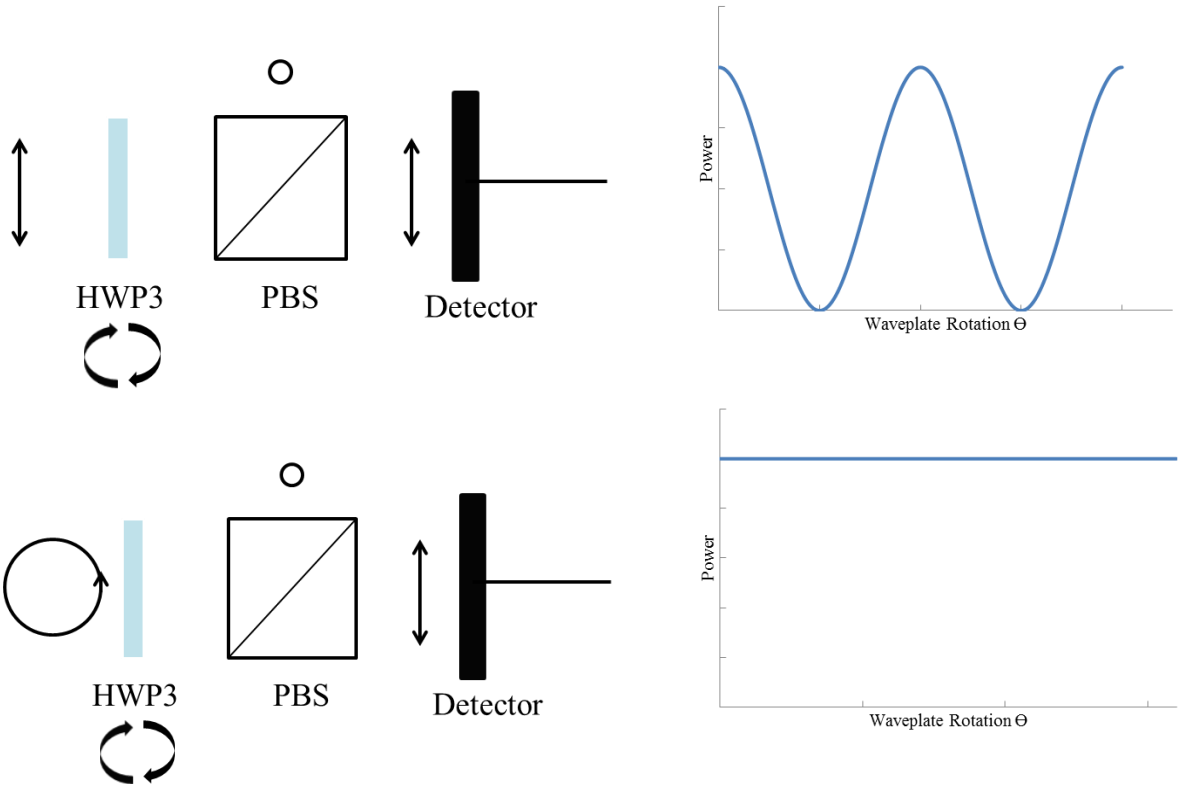

Figure 2.1 A top down view of the visibility measurement scheme. Using two polarizing optics, the degree of polarization can be quantified for the pump. The half wave plate (HWP3) rotates the state of polarization of the field by some angle. The analyzer (PBS) separates out the vertical and horizontal components. If the pump is linearly polarized, then the depending on the state of HWP3, at the maximum points the pump is either fully transmitted or coupled out, as indicated in by the power versus waveplate rotation plot.

Lasers

Lasers (light amplification by stimulated emission radiation) emit light that is coherent, monochromatic, and low divergence. The main components of a laser are the gain medium, the cavity, and the energy source. As light resonates in the cavity, it passes the gain medium many times. The atoms in the gain medium become excited. When the excited atom returns to the ground state due to no external influence, a photon is emitted, called spontaneous emission. However, when the excited atom interacts with another photon with the specific energy levels, the atom can be induced to emit a photon in phase with the incident or stimulated photon, hence stimulated emission. If the rate of production of photons exceeds the rate of loss of photons then the system will produce laser output. The cavity of the laser typically consists of a highly reflective mirror and a semi-reflective mirror to allow for output coupling.

Mode-locking

Lasers can have two types of output operation, continuous wave (cw) or pulsed (mode-locked). Although laser light is considered pure, it may consist of many different frequencies with varying degrees of phase coherence. In cw operation, the interference between the fields in this configuration induces intensity fluctuations and averages out to almost constant output intensity. In mode-locked operation, the phases of the fields inside the laser cavity are fixed so that periodically the fields would interfere constructively and destructively, leading to a periodic burst of light. Typically FOPOs are built with mode-locked lasers to ensure that a high peak power can be delivered to generate FWM. Continuous wave lasers have been implemented for FOPOs, but they are not ideal for biological applications. Mode-locked sources can deliver high peak power to a sample with low average power because the energy is compressed into short bursts which in principle should improve the signal to noise ratio for microscopy and spectroscopy measurements.

There are two types of methods to mode-lock a laser, active and passive. In the active mode-locking method, a modulator placed inside the laser cavity is used to phase-lock the modes. When the modulator placed inside a cavity is driven with a current, a modulation of the amplitude occurs. This generates sidebands at $v \pm f$. If the modulator frequency is the same as the cavity mode spacing, the sidebands will be phase locked with the central mode. In the passive mode-locking method, a saturable absorber is used to produce pulses. A saturable absorber is an optic that has intensity dependent transmission. In a passive mode-locking setup the saturable absorber would absorb low intensity light and transmit sufficiently intense light, and after many passes through the cavity a buildup of pulses can be generated.

Pulse Propagation through a Fiber

The propagation of light through a fiber can be derived from Maxwell's Equations, equations for magnetic and electric flux density, and the general expression for polarizability of a material. A detailed derivation can be found in [5] Figure 2.2 summarizes the equations used for deriving a generalized form of the wave equation to incorporate linear and nonlinear polarizations.

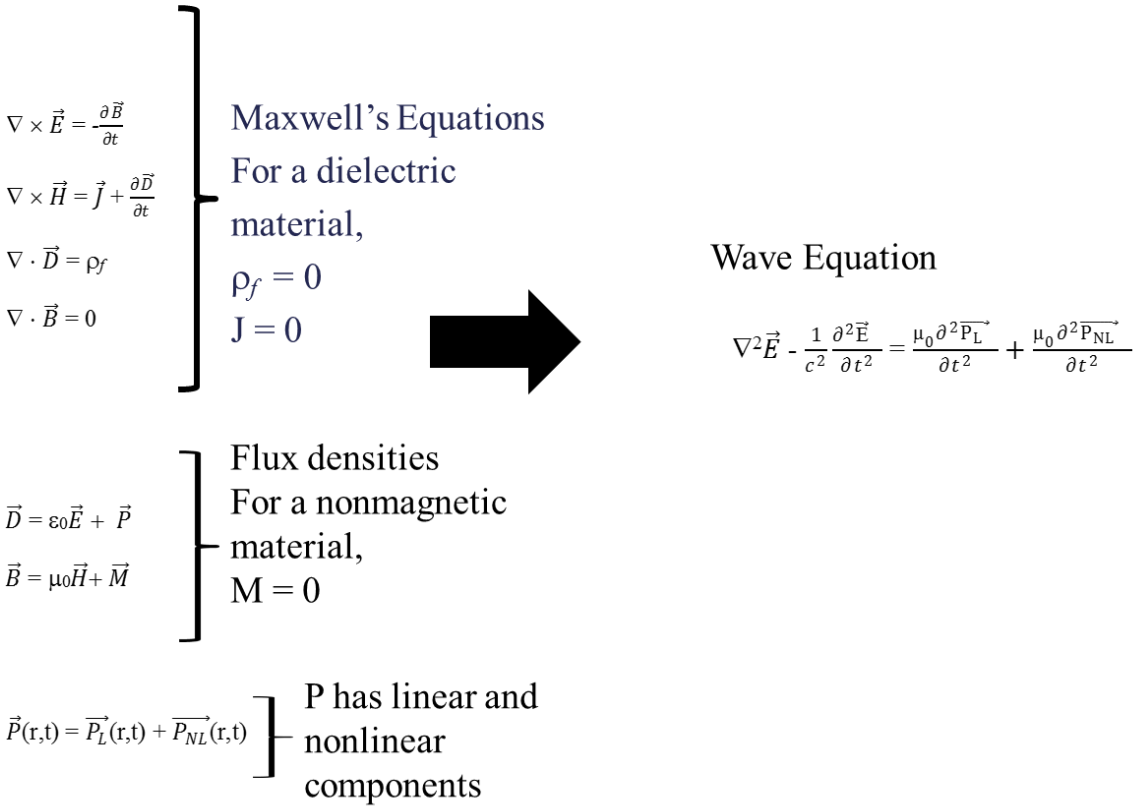

Figure 2.2 A summary of equations used for finding the pulse propagation equation.

$\vec{E}$ is the electric field vector, $\vec{H}$ is the magnetic field vector, $\vec{D}$ is the electric flux density, $\vec{B}$ is the magnetic flux density, $\vec{J}$ is current density vector, and ρ_f is the charge density. For optical fibers, J and ρ_f are equal to 0 because there are no free charges under normal conditions for SiO_2 [5]. The flux densities that respond to electric and magnetic field, $\vec{D}$ and $\vec{B}$, are related to $\vec{E}$ and $\vec{H}$, where $\vec{P}$ and $\vec{M}$ are the induced electric and magnetic polarization respectively, ε_0 is the vacuum permittivity and μ_0 is the vacuum permeability. In optical fibers $\vec{M}$ = 0 since SiO_2 is non-magnetic. The derived wave equation assumes the fields are plane polarized.

$$\nabla^2\vec{E} - \frac{1}{c^2}\frac{\partial^2\vec{E}}{\partial t^2} = \frac{\mu_0\partial^2\overrightarrow{P_L}}{\partial t^2} + \frac{\mu_0\partial^2\overrightarrow{P_{NL}}}{\partial t^2} \qquad (2.5)$$

The wave equation characterizes light traveling through a dielectric material, in which there are linear and nonlinear polarizations induced by the electric field.

Dispersion

Major considerations must be made for dispersion in fibers. Dispersion is the concept that electromagnetic waves of different frequencies travel through a material at different velocities. As the electromagnetic wave interacts with the electrons in a dielectric material, the absorption of the photon will be dependent on the energy at which

the bound electrons resonate [5]. As a result, the refractive index is related to the frequency of light interacting with the material.

Fiber dispersion is important to consider for the propagation of short pulses because different spectral portions of the pulse travel at different speeds as determined by $\frac{c}{n}$. The effects of fiber dispersion can be expressed as [5]:

$$\beta(\omega) = n(\omega)\frac{\omega}{c} = \beta_0 + \beta_1(\omega-\omega_0) + \frac{1}{2}\beta_2(\omega-\omega_0)^2 + \ldots \quad (2.6)$$

$$\beta_1 = \frac{d\beta}{d\omega} \ , \ \beta_2 = \frac{d^2\beta}{d\omega^2}$$

where β is the propagation constant of the guided mode within the fiber, n is the refractive index, and ω is the frequency of the participating fields. β is related to the free space propagation constant k by [18]:

$$\beta = n_{eff}k = n_{eff}\frac{2\pi}{\lambda} \quad (2.7)$$

The first derivative of β with respect to frequency yields the group velocity, according to

$$\left(\frac{d\beta}{d\omega}\right)_{\omega_o} = \frac{1}{v_g(\omega_o)} \quad (2.8)$$

which can be described as the overall velocity of the propagating pulse. The second derivative of β with respect to frequency yields the dispersion of the group velocity [5]. A pulse traveling through a fiber moves at the group velocity as determined by β_1, while β_2 governs pulse broadening. The frequency where β_2 disappears is known as the zero dispersion wavelength of the fiber. It is ideal to operate a FOPO near this regime because the required phase matching conditions for efficient FWM are easier to satisfy. Phase matching will be discussed later on. Another form of dispersion is polarization mode dispersion. Fibers have an optimum acceptance and propagation for the state of polarization of the input light. In some fibers, variations in the fiber core cause the propagation constant to differ for modes polarized in the x and y directions. This is called modal birefringence [5]. As a result, light propagates at different velocities in each axis. The fast axis is where the light propagation experiences a larger group velocity than in the slow axis. If an input pulse has a polarization state that excites both x and y polarization components, then the pulse becomes broader at the output due to variations in the group velocities, this is called polarization mode dispersion.

Fiber Optics

The FOPO can be thought up as a laser that is pumped by another laser. Typical optical fibers are made of a glass core that is surrounded by a cladding. The refractive index of the cladding is lower than of the core, which allows for light to travel through the fiber through means of total internal reflection. Fibers can be designed to be either polarization or non-polarization maintaining [10]. In polarization maintaining fibers, the fiber is fabricated to have two axes with different refractive indices. If the light launched into a PM fiber has a state of polarization parallel or linear to the x or y axis, then the

polarization is maintained. In a non PM fiber, the core of the fiber has a circular geometry, resulting in no associated birefringence in either axis. The state of polarization changes as light propagates through a non PM fiber, requiring that the state of polarization must be controlled throughout the oscillating cavity.

Photonic Crystal Fibers

Nonlinear optical phenomena are undesirable in communications because the signal traveling through the fiber can get degraded. However, for designing novel parametric devices the nonlinearity can be utilized. To increase the nonlinearity of a fiber, the fields traveling down the fiber must have sufficient interaction; one can increase the length of the fiber to hundreds of meters and or decrease the relative core size. In this thesis we use a unique fiber called a photonic crystal fiber (PCF). A schematic of the front face of a typical PCF is given in Figure 2.3. The PCF's glass core is surrounded by a cladding of air holes arranged in a periodic pattern. The air hole design allows for guidance properties that could not be attained in standard fiber, such as designing a smaller core for maximizing nonlinear optics or to shift the zero dispersion wavelength [27]. The reduction in the core size increases the nonlinearity of the fiber, as the nonlinearity is inversely proportional to the effective area of the core [25]. The properties can be further tailored by adjusting the diameters of the holes, D, or the spacing between each hole, Λ. PCFs are unique in the sense that the zero dispersion wavelengths can be shifted from 1200 nm range to the visible range.

(a) (b)

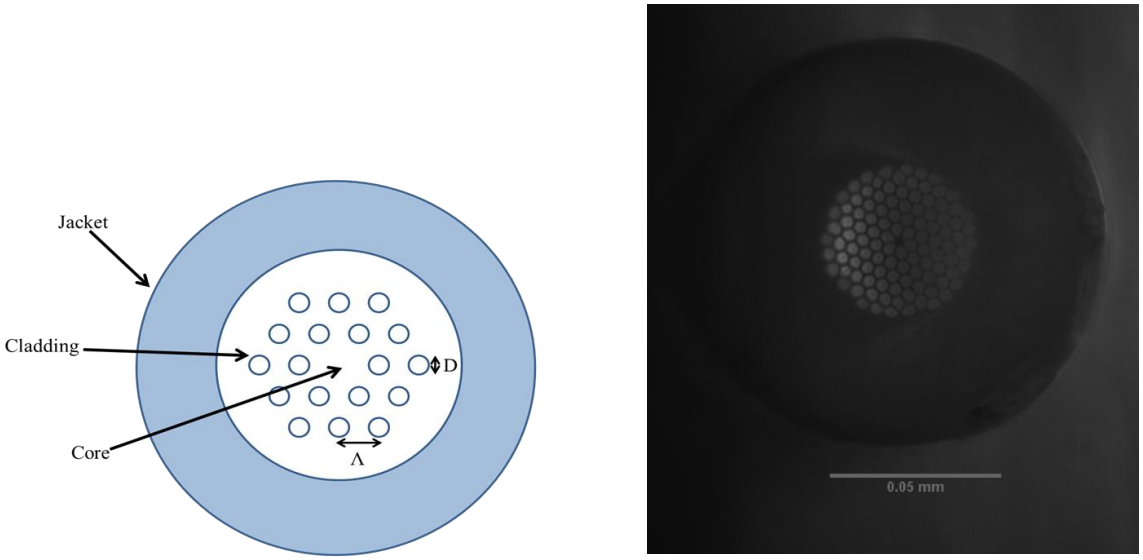

Figure 2.3 (a) A schematic of a PCF. The properties of the fiber can be tailored by varying the air hole spacing Λ, the diameter of the holes D, and the pattern of holes. (b) An image of the front face of a PCF with 40x magnification.

Nonlinear fiber optics

When an electromagnetic field interacts with a material, a polarization P results from the induced electric dipoles. This can be expressed as:

$$\vec{P} = \varepsilon_0(\chi^{(1)}\vec{E} + \chi^{(2)}\vec{E}\vec{E} + \chi^{(3)}\vec{E}\vec{E}\vec{E}) \quad (2.9)$$

where ε_0 is the vacuum permittivity and χ is the susceptibility of the material [5]. The term χ refers a set of matrices that describe the optical properties of a material with the interaction of incident light. Nonlinear optical phenomena occur for terms $\chi^{(2)}$ and higher. From equation (2.7), it can be inferred that nonlinear optics occurs for high intensity fields. Optical fibers, due to the isotropic nature of SiO_2, normally express $\chi^{(3)}$ processes rather than $\chi^{(2)}$ processes [5] but experimentally $\chi^{(2)}$ processes have also been observed due to imperfections in fiber fabrication. The pulse propagation equation derived from Maxwell's equations assumes that the participating fields are all copolarized, which translates to χ being a scalar quantity. In practice, the participating fields will usually not be copolarized unless if one is using polarization maintaining fibers.

The $\chi^{(3)}$ response gives rise to an intensity dependent refractive index. This is often written as:

$$n = n_o + n_2 I \quad (2.10)$$

where n is the effective refractive index, n_o is the initial refractive index, n_2 is the nonlinear refractive index, and I is intensity of the applied field. The nonlinear effects that we are interested in are self-phase modulation, cross-phase modulation, and four wave mixing.

For a single beam, a nonlinear effect called self-phase modulation (SPM) can occur. SPM is defined as a self-induced phase shift due to an optical field's own intensity. In the case where there are multiple beams present, cross phase modulation (XPM) occurs. XPM is defined as an induced phase shift due to the modulation of the refractive index by two different electromagnetic fields. Both SPM and XPM occur concurrently [5]. We utilize SPM and XPM in the process of operating our FOPOs because they occur simultaneously with FWM.

Four wave mixing theory

Four wave mixing (FWM) is the interaction between three fields to generate a new fourth field at a different frequency. FWM is a third order process and can be studied from the third order polarization term:

$$\vec{P}_{NL} = \varepsilon_0\chi^{(3)} \vdots \vec{E}\vec{E}\vec{E} \quad (2.11)$$

There are two types of four wave mixing, non-degenerate, in which all of the fields are different frequency, and degenerate, where two of the fields have the same frequency [5].

For this thesis the only the degenerate case is considered because our FOPOs are pumped from a single source.

One can first visualize two waves at ω_1 and ω_2 copropagating in a fiber. As they move through the fiber, the two fields will beat with each other, modulating the refractive index of the fiber and generating a new frequency at ω_3. When another field ω_3 is added, ω_3 could beat with ω_1 and modulate ω_2 or beat with ω_2 and modulate ω_1. In the case of modulating ω_2, sidebands will be generated at $\omega_2 \pm (\omega_3 - \omega_1)$. This will coincide with other generated sidebands. The beats in the electromagnetic waves will modulate the refractive index of the fiber, which will allow for the generation of more sidebands and sum and difference frequencies between the participating fields. The effect can lead to a gain in the signal [19].

In the quantum-mechanical approach for the degenerate case, two pump photons at frequency ω_p are eliminated while two photons at ω_s and ω_i are generated. Efficient FWM occurs when the two conditions are met:

$$2\omega_p = \omega_s + \omega_i \tag{2.12}$$

$$\Delta\beta = \beta_s + \beta_i - 2\beta_p = 0 \tag{2.13}$$

Equation 2.10 corresponds to an energy conservation in which two pump (ω_p) must equal to the energy of the generated signal (ω_s), and idler (ω_i). Equation 2.11 corresponds to a momentum conservation in which the propagation of two pump fields (β_p) and the propagation of signal (β_s) and idler fields (β_i) should have a phase mismatch of 0 for efficient FWM. To satisfy the requirements of phase matching the dispersion properties of fiber must be tailored to the pump source.

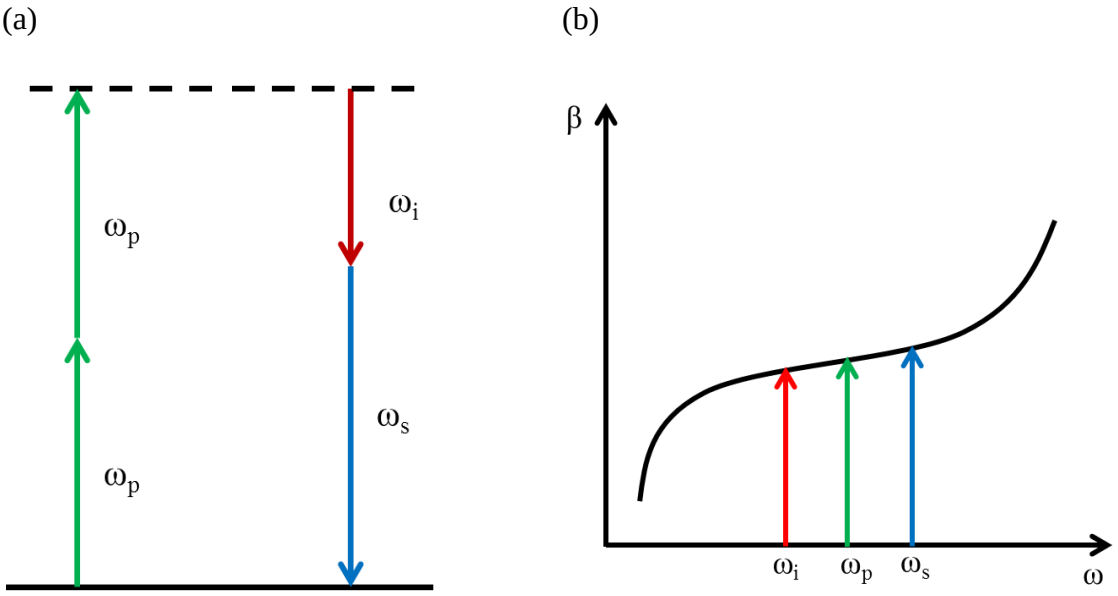

Figure 2.4. Energy (a) and phase matching (b) diagrams depicting the requirements for FWM. In the quantum mechanical picture two pump photons (ω_p) are eliminated to generate a photon at lower frequency (ω_i) and higher frequency (ω_s). Another requirement is that the propagation vectors of the signal and idler must equal to twice of the pump.

For copolarized pump, signal, and idler fields we can use scalar FWM theory. However, in practical applications the polarization of the participating fields will not completely align unless if one is using a polarization maintaining fiber. The χ term will change, which dictates the interplay between the induced polarization of the material by light and the state of polarization by the incident light. In one of our FOPO characterizations we use a non PM fiber, which complicates our understanding of the FOPO.

Gain for the Signal Field

Using equation (2.5), one can derive an expression for the complex field amplitudes for pump, signal, and idler, also known as the coupled amplitude equations. Details of the derivations can be found in [5] and [10]. Figure 2.5 summarizes the equations utilized for finding an expression for gain in a FOPO system. Looking at the coupled amplitude equation describing the propagation of the pump field [19]:

$$\frac{\partial A_p}{\partial z} = i\gamma[(|A_P|^2 + 2(|A_s|^2 + |A_i|^2))A_p + 2A_sA_iA_p^*\mathrm{e}^{(i\Delta\beta z)}] \tag{2.14}$$

we can note some interesting nonlinear effects. The first term $|A_P|^2$ is SPM. The second term $2(|A_s|^2 + |A_i|^2)$ is XPM. The third term $2A_sA_iA_p^*\mathrm{e}^{(i\Delta\beta z)}$ is FWM. The nonlinearity coefficient, γ is given as:

$$\gamma = \frac{n_2\omega_p}{A_{eff}c} \tag{2.15}$$

where n_2 is the nonlinear refractive index, ω_p is the frequency of the pump, A_{eff} is the fiber core diameter, and c is the speed of light. The term determines the nonlinearity of the fiber. PCFs are ideal for nonlinear optics because the A_{eff} of the fiber can be greatly reduced, increasing the nonlinearity coefficient.

From the coupled amplitude equations, one can make an assumption of a large pump field and a small signal field, which suggests that the pump field does not change (dA/dz = 0) and the signal field at the input does not affect pump field. A summary of equations used to derive the power of the signal is listed in Figure 2.5. The conversion efficiency, or gain, of the signal G_s can then be expressed as [19]:

$$G_s = \frac{P_s(L)}{P_s(0)} = 1 + \left[\frac{\gamma P_p}{g}\sinh(gL)\right]^2 \tag{2.16}$$

Equation 2.14 indicates that the gain for the signal field depends on the gain coefficient g, the length of the fiber L, the pump power, and the nonlinear coefficient γ [19].

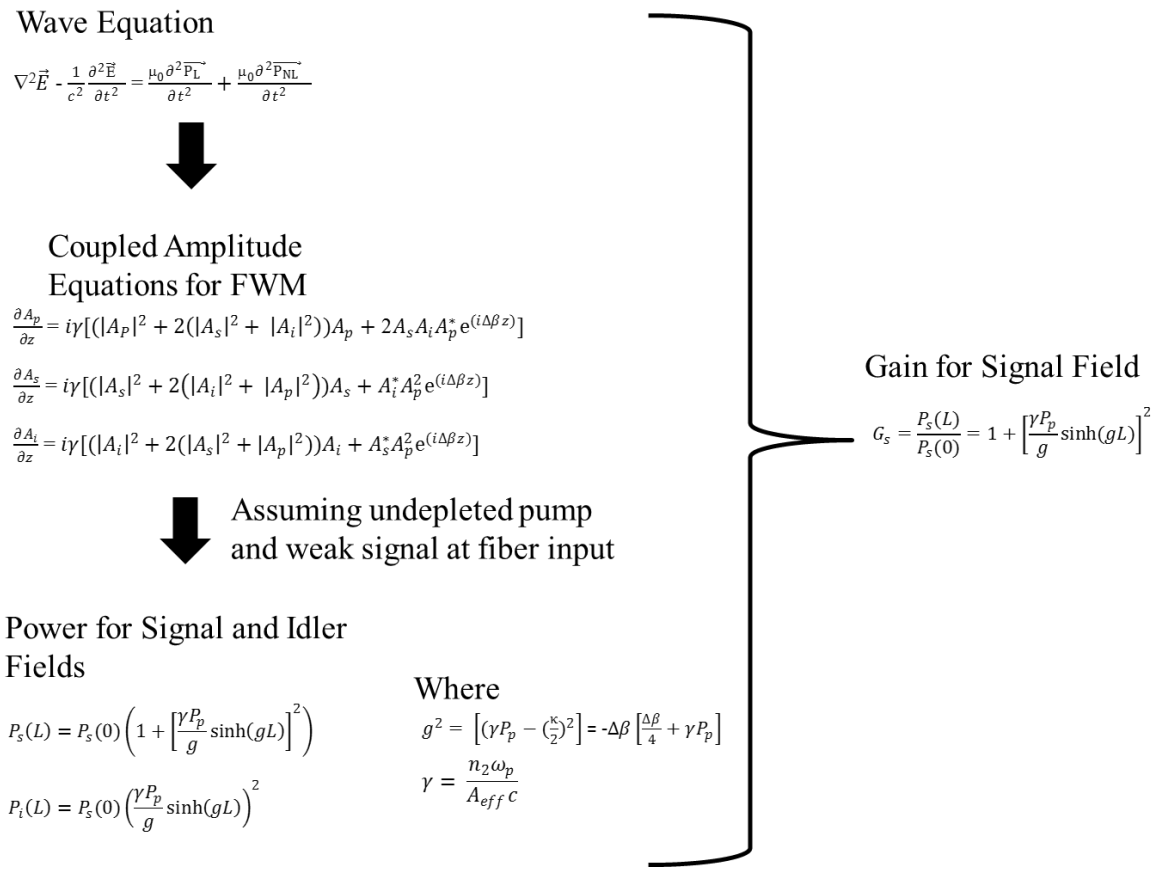

Figure 2.5. Summary of equations for determining the gain for the signal and idler fields [19]. The pump field is assumed to be undepleted, meaning that the pump intensity is assumed to have no change during the parametric process. A corresponds to the amplitude fields for pump (p), signal (s), and idler (i), Δβ is the propagation constant, γ is the nonlinearity coefficient, and g is the parametric gain coefficient. By taking the ratio between $P_s(L)$ to $P_s(0)$, one can determine the conversion efficiency for the signal field, G_s.

FOPO Operation

When pump pulses propagate through the fiber, the nonlinearity of the fiber leads to spectral broadening of the pump pulses due to self-phase and cross-phase modulation. We can use this observation to determine if FWM is also occurring since they occur under the same conditions. Sidebands will be generated as a result of FWM. An end mirror can be placed at the output of the fiber to build an oscillator. A dispersive element is placed at the output of the fiber as a spectral filter such that a narrow (~3 nm) band of light is fed back into the fiber. When the optical path length of the cavity is synchronized with the pump pulse train another pump pulse interacts with the fed back portion of the spectrum, resulting in an amplified signal and the generation of an idler field. The amplification process continues until a steady state is reached, in which the system will emit laser-like output. With high enough gain the FOPO can tolerate high losses and still be operational [25]. Under these conditions the FOPO operates where FWM dominates

over other nonlinear effects such as Supercontinuum generation or stimulated Raman scattering [21].

FOPOs versus traditional lasers

FOPOs and traditional lasers both have coherent output. However, the method of gain differs between the two systems. In lasers, the gain can be described as transitions to discrete energy levels, while in FOPOs the gain is determined primarily by phase matching. The difference in the gain affects the operation of each system. For traditional laser system one would typically operate in low output coupling ratio to lower the loss in the cavity. For FOPOs, the highest output powers correspond to higher output coupling ratios [22].

FOPOs versus FOPAs

A very similar device to FOPOs is the fiber optical parametric amplifier (FOPA). A FOPA has only one pass in through the fiber, while a FOPO has multiple passes. FOPAs have already been utilized for performing CRS microscopy. FOPAs are attractive since they do not require cavity synchronizations, resulting in a simpler mode of operation compared to an oscillator. However, FOPOs have a couple of advantages. First, due to the multi pass nature in a FOPO leads to more output power in comparison to a FOPA. Second, many FOPA sources require a second laser to provide the seed for wavelength conversion; in FOPOs the system can be pumped by a single laser. Third, the tunability of a FOPA would be determined by tuning either the seed or pump laser wavelength; certain types of FOPOs can be tuned by adjusting the wavelength of the pump or adjusting the dispersive element in the cavity for small wavelength changes.

Chapter 3

Polarization-Dependent Output Coupling

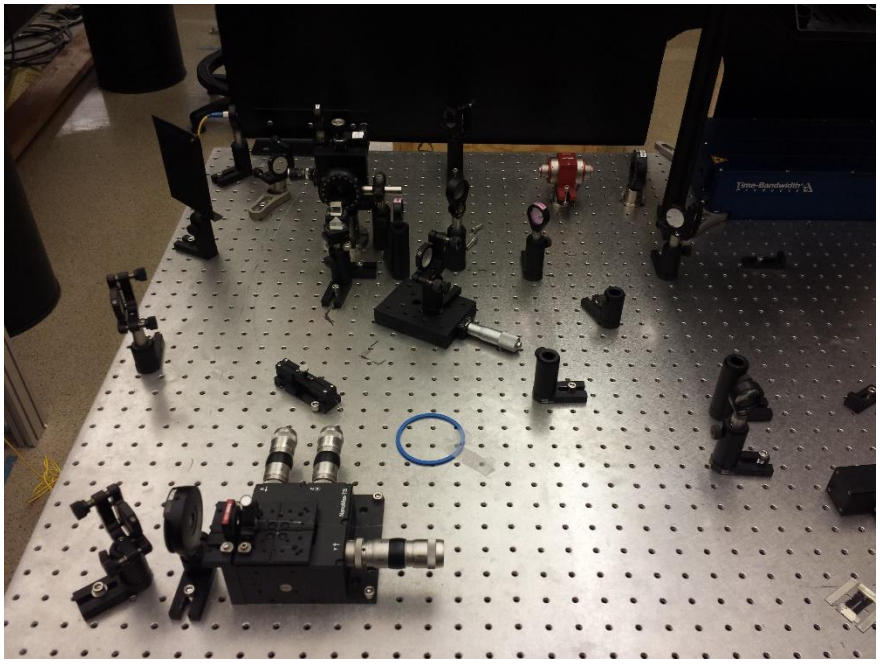

Figure 3.0 The layout of the Nd:YVO_4 pumped FOPO.

Introduction

In this chapter we describe a Nd:YVO_4 pumped FOPO system in which we tailor the output coupling through polarization optics to optimize for output power. One of the main drawbacks in FOPOs in comparison to solid state OPOs are low output powers and limited tunability [10].

There have been several recent developments in FOPO design and optimizations for improved performance. Xu et al., designed a multi-watt FOPO based on dispersion-shifted fibers in which the output power was maximized by choosing the optimum feedback fraction for a given input pump power [21]. Murray et al., utilized gain-switched diodes as the seed source for a tunable FOPO system [23]. The methods used for FOPO optimization usually involve tailoring the pump source or the fiber. A recent publication by Jin *et al*. determined that the highest output powers in FOPOs are achieved with high output coupling ratios close to 1 [22]. Their study did not consider the effects of polarization in output coupling.

Typically one would tailor the fiber to improve FWM processes, which would directly lead to an increase in output power. However, we propose to tailor the output coupler to extract more power from the cavity while maintaining a working FOPO. FWM is polarization dependent but the fiber we use for this system is not polarization maintaining, suggesting that the state of polarization from the input of the fiber to the end mirror must be carefully tailored with polarization optics. We find experimentally that using a polarization-based output coupling scheme (half-wave plate (HWP) and polarizing beam splitter (PBS)) with this system provides essential flexibility in adjusting the output power coupling ratio while maintaining stable operation. We observe a symmetric and an asymmetric output coupling waveform depending on the configuration of the polarization optics, which can produce up to 100 mW and 140 mW respectively in total sideband power. By modifying the polarization state at the fiber output to asymmetric conditions, we can achieve an increase of (25% ± 5%) output power, which is illustrated in our simulations. Polarization based output coupling supplements the need for controlling the state of polarization at the output of the fiber and the feedback**.** Our simulations confirm that we obtain the high output power for the case where the polarization state of the oscillating mode within the FOPO cavity is adjusted to overlap with that of the pump polarization mode within the FOPO cavity.

Experimental Description

The FOPO consists of a 1.2-m long microstructure fiber (NKT Photonics, NL 5.0 1065) pumped by a mode-locked 1064nm Nd:Vanadate laser (Time Bandwidth, 800 mW output power, 80 MHz repetition rate, 8 ps pulse duration). The reflections from the front cleave of the fiber and the end mirror form a Fabry-Perot cavity. This method of designing a cavity leads to loss of energy greater than 95% [20]. FOPO tuning occurs by adjusting both the angle and position of the end mirror. Our 8-ps-pumped microstructure-fiber based FOPO has 75% of the cavity fiber guided. Free-space elements accomplish output coupling, spectral filtering, and cavity synchronization. A significant portion (~80%, 70 mW) of energy from each of the sidebands is coupled out using a polarization-

based output coupler. The wavelength tuning range is from 960-1044 nm on the signal side and 1084-1191 nm on the idler side. The wavelengths for peak operation are 992 nm and 1147 nm. Output pulse durations are 2.2 ps. Our microstructure fiber is non-polarization maintaining. Lacking clear polarization modes it is difficult to determine the ideal input pump polarization and to understand the polarization dynamics within the FOPO. We use two FOPO output coupler variations in these experiments: a polarization dependent and independent version.

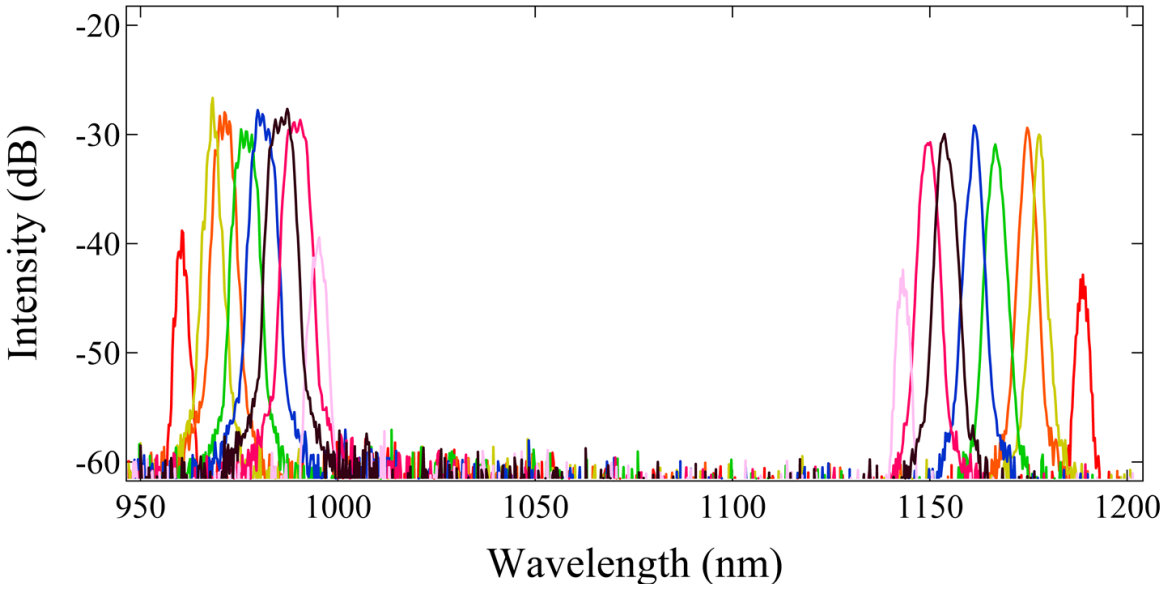

Figure 3.1 A tuning plot of the Nd:YVO_4 FOPO system. The pump is at 1064 nm (not shown in the tuning plot)

Polarization Independent OC

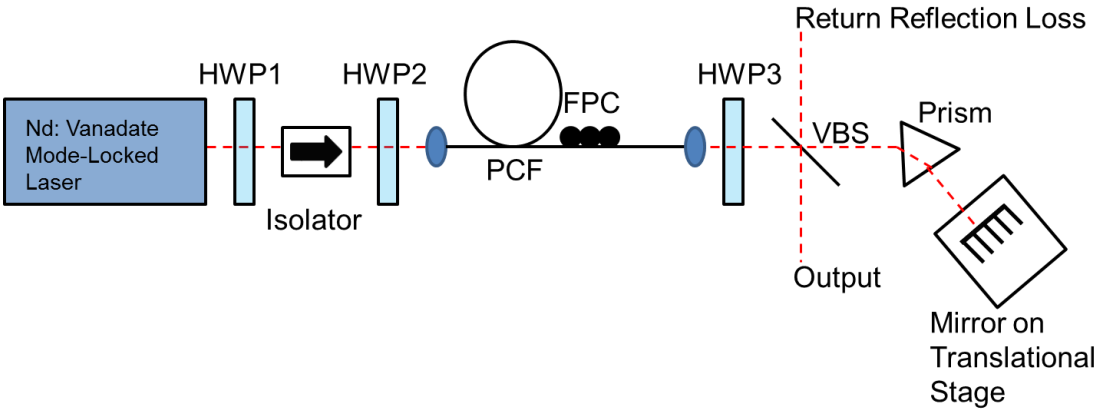

Figure 3.2 Schematic of the polarization independent output coupling.

A schematic of the polarization independent output coupling system is given in Fig 3.2. Aspheric lenses at the input (Thorlabs C220 TME-C) and output (Thorlabs C110TME-C) are used for coupling of the pump and feedback into the fiber. HWP1 (Thorlabs WPH05M-1053) and the isolator control the input pump power into the fiber. We use a variable beam splitter (Thorlabs NDC-50C-4M) as the output coupler. Although the output coupler is a simple reflection, the polarization state is adjusted by HWP2, fiber polarization controller (Thorlabs PLC-900), and HWP3 for optimum transmission through the prism. There is a return reflection loss due to a second pass through the VBS leading to an additional contribution to FOPO cavity losses comparable to the output coupling ratio. The output coupling ratio was varied by rotating the VBS. The output power as a function of reflectivity, or the output coupling ratio, was measured for several different pump powers. Reflectivity, R was calculated by the equation:

$$R = 1 - T \tag{3.1}$$

T is the ratio between the powers transmitted through the PBS and at the output of the fiber. We could have directly measured the reflectivity by simply taking the ratio between the amount of pump powers reflected out by the PBS and at the output of the fiber, but we have observed some reflections due to the imperfections of the PBS. Therefore we thought it would be more accurate to measure transmission since the calculation would factor in more losses. The reflectivity plot is given in Figure 3.3.

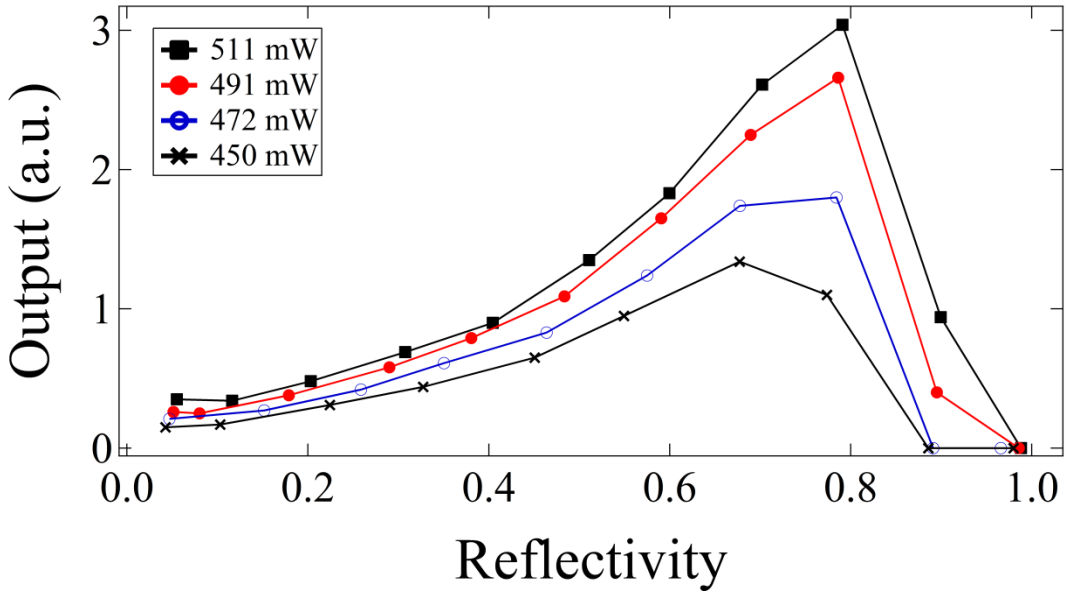

Figure 3.3 A plot of the output power (in arbitrary units) versus the output coupling ratio

We note that the for high input pump powers, the output power increases for increasing reflectivity, meaning that for higher input powers, we can output couple more power. This has been observed experimentally in [21, 22]. We find that the FOPO can function under high output coupling ratios and oscillate even under high losses. This is a

noticeable contrast in comparison to solid state or fiber laser systems, where one would like to output couple as little as possible [22].

Even though this system can function well, we believe that we can optimize the system further. The VBS output coupler has numerous drawbacks. First, there is a return reflection loss from the feedback because we cannot control the state of polarization from the feedback. Second, the feedback polarization state cannot be assumed to be well overlapped with the polarization state of the pump through the fiber, which can reduce FWM gain. We believe we can address this issue through using a polarization dependent output coupler.

Polarization Dependent Output Coupling

A schematic of the polarization dependent output coupling system is given in Figure 3.4. Since the output coupler has been changed to a polarizing beam splitter (CVI Laser Optics, PBSH 450-2000-05) the output coupling dynamics differ compared to the system described in Figure 3.2. At the output of the fiber, HWP3 controls the polarization incident on the PBS, and thus controls the output coupling ratio. Adjustments to HWP3 also change the state of polarization of the field fed back into the fiber. One adjustment scenario is to set the polarization optics to achieve maximum polarization overlap between the pump and the oscillating signal fields. The PBS separates horizontal and vertical components of the light from the fiber output, with horizontally polarized light transmitted through the polarizer and vertically polarized light reflected out of the cavity. By adjusting HWP2, FPC, and HWP3, one can determine the ratio of transmitted and output coupled light. For example, one can adjust the system so that very little light is coupled out. In this case the cavity loss is relatively low and the FOPO can be easily adjusted to be above threshold for operation. Unfortunately, not much power is coupled out. Conversely, when the output coupling ratio is high, the FOPO will not operate since not enough light is fed back into the fiber for the parametric process. Output power as a function of PBS reflectivity is then recorded for several FOPO pump powers.

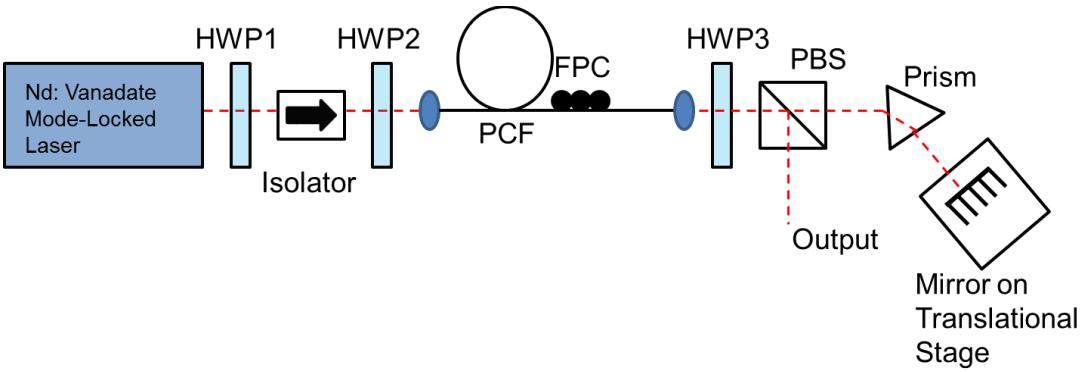

Figure 3.4 Schematic of the polarization dependent output coupling.

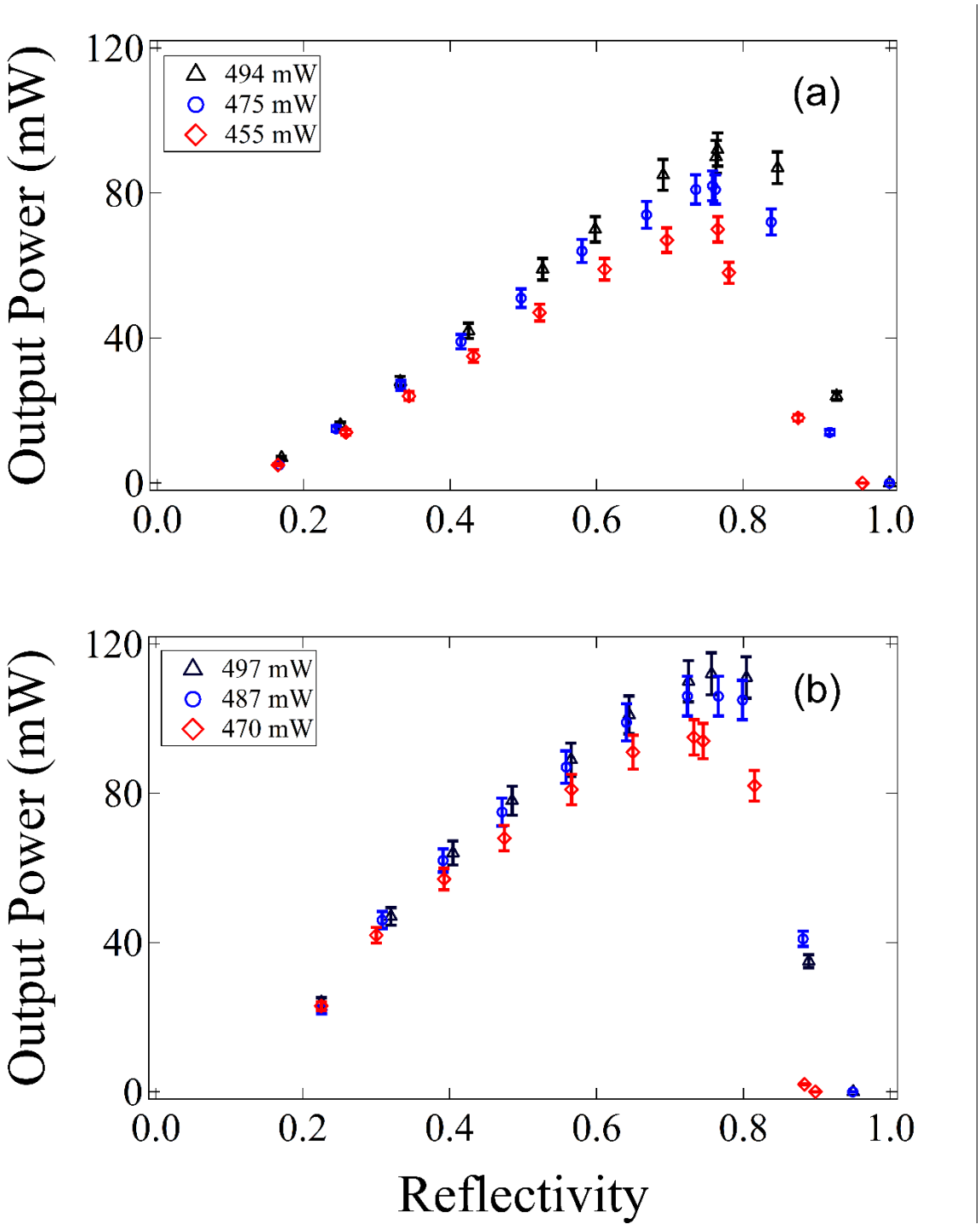

Figure 3.5 Reflectivity measurements of the polarization dependent output coupling scheme for symmetric (a) and asymmetric (b) cases. As the input power to the FOPO increases, the reflectivity for optimum output power also increases. The optimum reflectivity for both scenarios is between 0.7 to 0.8.

For our polarization-dependent measurements we mounted HWP3 on a motorized rotating stage to rapidly measure output power based on changing polarization states at the output of the fiber. The FOPO output (pump, signal and idler) was recorded on an oscilloscope for waveform analysis. The pump field is seen to be plane polarized by observing the sinusoidal variation in power having a visibility >0.9.

Figure 3.5 represents the output power as a function of output coupler reflectivity for various pump powers for two different FOPO operation scenarios which we call *asymmetric* and *symmetric* conditions. Figure 3.5 (a) illustrates output coupling ratio for symmetric conditions, while Fig. 3.5 (b) is for asymmetric conditions. The range of optimum output coupling corresponds to reflectivities of 0.7-0.8 for both scenarios which is in agreement with the results in [22]. Note that we obtain a larger maximum output power in the asymmetric case. We observe that the reflectivity for optimum output power increases for increasing input pump powers. However, similar reflectivities yield different output powers depending upon the configurations of the polarization optics. This indicates that reflectivity alone does not determine optimum FOPO operation

To aid in clarifying the role of polarization, we mounted HWP3 on a motorized rotating stage to rapidly measure output power based on changing polarization states at the output of the fiber. The FOPO outputs (signal and idler) were recorded on an oscilloscope for waveform analysis. We observe the FOPO output waveform as we adjust the polarization state of the pump pulses propagating through the fiber by varying FPC and HWP2. Figure 3.6 illustrates two measurements of the output power of the FOPO as a function of waveplate (HWP3) orientation. In Fig. 3.6 (a) we see that the signal and idler have essentially overlapping waveforms and each of the four peaks is roughly the same height. In the section labeled “I”, we observe a flat region of the curve indicating that FOPO is not operational. In region “I”, the output coupling ratio is too large and cavity losses are too high that the FOPO is below threshold. As the HWP3 angle increases the oscillation threshold is reached in the region labeled “II”, and the output power increases dramatically. The output then reaches a maximum at “III” and begins to decrease. Due to the imperfections in the PBS, the output coupling ratio reaches a minimum of about 4% and we see a smoothly varying dip labeled “IV” in the output power corresponding to low output coupling and low output power. Here the FOPO is above threshold, but not much power is directed out of the system. As the HWP3 angle increases further, the output power increases once again in a similar fashion and reaches another maximum (“V”) that is comparable in power to the first peak. A maximum of roughly 50 mW in each sideband could be generated in the symmetric case.

If we adjust HWP2, FPC, and HWP3 to maximize the output power and then record the output power as a function of HWP3 angle the trace becomes asymmetric. In this case (shown in Fig. 3.6(b)) a small peak in output power occurs near $\pi/2$ (I) and a larger peak occurs at around $3\pi/4$ (II). The asymmetric mode of operation delivers roughly $(25 \pm 5)\%$ more output power than the symmetric mode. The pump field is still linearly polarized in this case except with a slightly lower visibility. Roughly 70 mW in each sideband is generated with the polarization dependent asymmetric case.

We find that the FOPO can be adjusted to oscillate for a wide variety of pump polarization states including plane and elliptical states. Adjusting the half-wave plates and FPC to obtain maximum output power does not necessarily leave the pump in a plane

polarization state. In fact, we observe output powers equivalent to our highest observed values for plane and elliptical pump polarizations. For the studies presented here we restrict our observations to the case where the pump is in a plane polarized state at the output of the fiber.

Adjusting HWP3, HWP3, and FPC all effect the output coupling ratio but one cannot simply use this ratio as a determinant for maximum output power. The polarization elements introduce the need to pay attention to polarization throughout the cavity. The polarizers in the FOPO system may be orientated in which the reflectivity would be optimum under a simple reflection, however the oscillating electric field direction after each pass may not align well with that of the pump field. If the oscillating fields do not overlap well with the pump field then the FWM gain will be reduced.

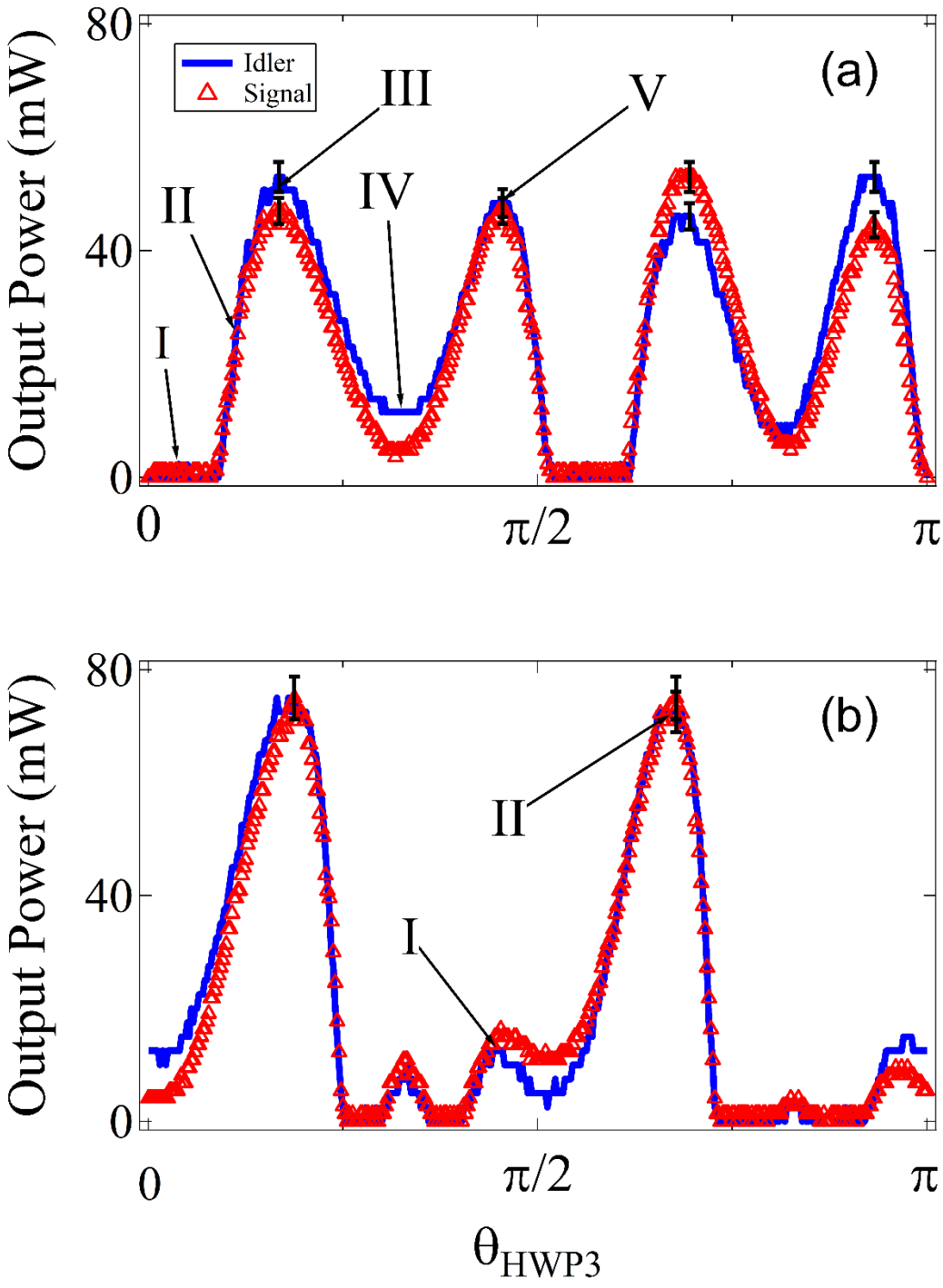

Figure 3.6 Output waveforms as function of HWP3 rotation. We observe two unique cases, a symmetric (a) and an asymmetric (b). The asymmetric case has roughly 20% more output power. As for the visibility, we are unable to conclude the optimum pump polarization state for best output power. We have observed that the FOPO can give optimum output coupling for both high (<0.9) and low (~0.5) visibilities. The key difference is that the output coupling waveforms differ.

Simulations

We simulate the output coupling polarization dynamics through the use of Stokes vectors in MATLAB. The code was written by Dr. Jay Sharping. In the code, a linear polarization state is first sent through a HWP, and then through a PBS. The orientation of simulated HWP determines how much energy is reflected out and how much remains in the FOPO cavity. Figure 3.7 summarizes the operation of the code. After the PBS, the field within the FOPO cavity is a horizontally linear polarized state which is reflected back through the same PBS. The horizontally linearly polarized field them passes back through the HWP. The resulting Stokes vector reveals the polarization state and can be used to calculate the loss due to cavity output coupling. We also calculate the projection of the resulting Stokes vector with that of the pump, giving a polarization overlap factor. The simulation is then repeated with many different configurations of the HWP. We assume that maximum parametric conversion occurs when the feedback polarization state matches and with the polarization state of the input.

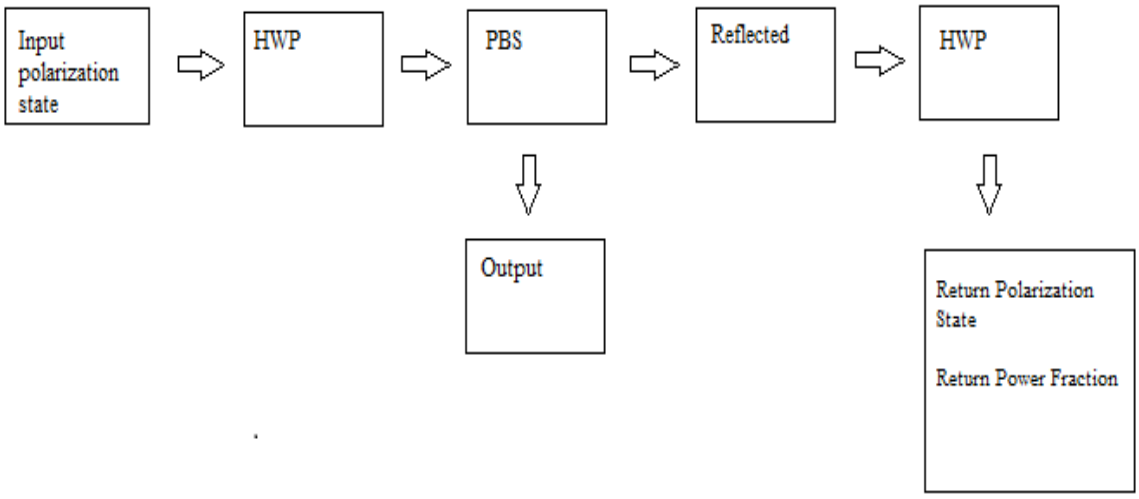

Figure 3.7 A summary of the FOPO simulations. Efficient FWM is determined by polarization mode overlap between the pump and feedback.

Poincare Sphere

The polarization modes can be visualized through the use of the Poincare sphere. Figure 3.7 gives a representation of the Poincare sphere. S1, S2, and S3 represent the Stokes parameters [24]. The Stokes parameters are another way to write the state of polarization of light and fitting it on a spherical coordinate. S1 describes the degree of linear horizontally polarized light over vertically polarized light; S2 describes the degree of linearly polarized $\pm 45^{o}$ light, and S3 describes the degree of right circularly polarized light over left circularly polarized light [24]. A detailed description and derivation of the Poincare sphere can be found in [18, 24].

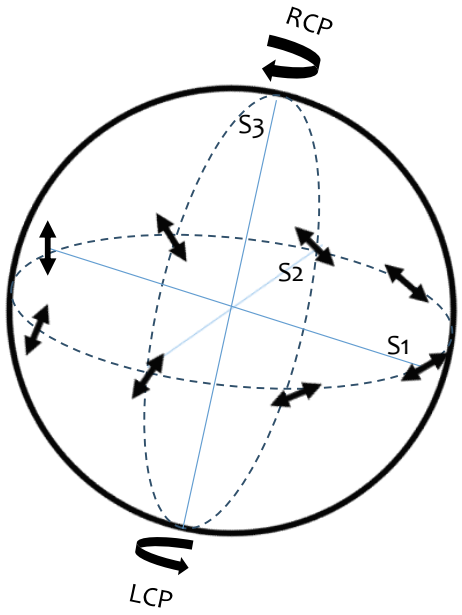

Figure 3.8 Schematic of the Poincare sphere. The Poincare sphere is a graphical representation of all the polarization states of light based off of the Stokes vectors. The equator of the sphere represents linear polarization states, the poles of the sphere represent circular polarization, and the rest of the sphere represents elliptical polarization. In our simulations the HWP changes the position of light on the equator. The PBS sets the state to S1 on the sphere.

For visualization of the state of polarization on the Poincare sphere, the input state of polarization is assumed to be linear, and therefore the positions are fixed onto the equator of the sphere. When the pump pulse moves through the HWP, the polarization changes by a determined angle, in which on the sphere shows that the position has changed on the equator. The input then passes through a polarizing beam splitter, which then would transmit horizontal components of the input, setting the position on the sphere to be S1. Feedback into the cavity is determined by HWP, in which the polarization state is rotated counter clockwise to the input. When the input state of polarization is vertical, horizontal, or $\pm 45^{o}$, this yields a symmetric case.

.

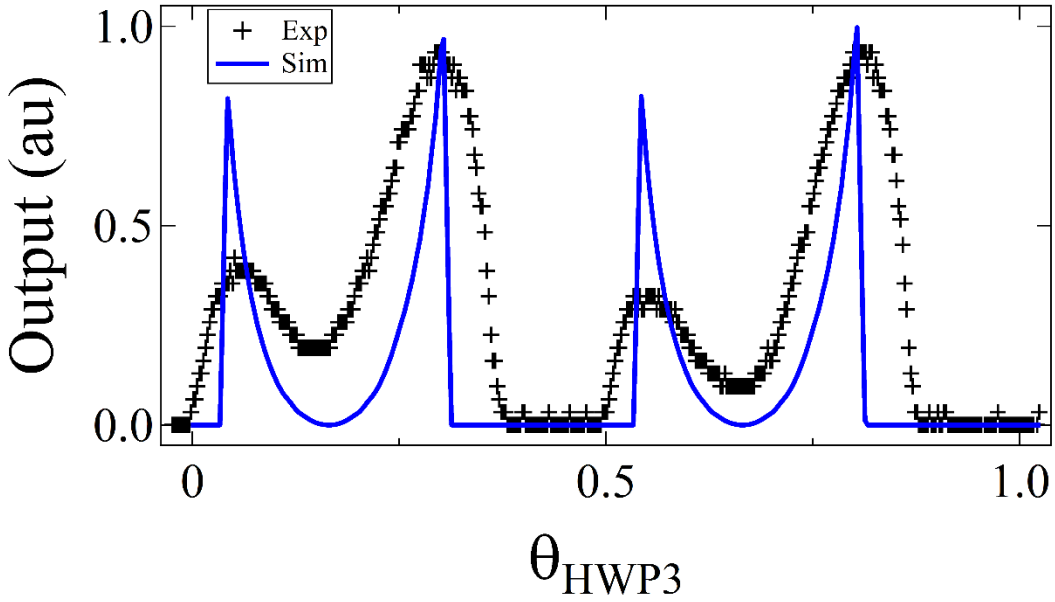

Figure 3.9 Comparison between relative experimental (black symbols) and simulated (blue line) output. Notice that the relative output narrows and the asymmetry becomes less pronounced when we factor in gain saturation. We did not factor in noise in our simulations, which may explain the shape of the curve.

Our experimental data is compared to simulated results in Fig. 3.8, which represents the case where the FWM gain saturation is included. We observe that the simulation captures an asymmetry, but that the imbalance is not as large as observed experimentally. In applying a gain saturation, we find that the simulated data becomes narrower and the asymmetry less dramatic. We expect that if we were to factor in other degradations comparable to experimental condition, the output curve would be similar to the observed experimental results.

Discussion

The output coupling of our FOPO can be greatly increased by adjusting polarization parameters. We observe a roughly 20% increase in the output power by adjusting polarization optics. Based on the orientations of the polarizers, the FOPO can be working in the symmetric mode, where there are more oscillating conditions at the cost of reduced output power or the asymmetric mode, where reduced oscillating conditions allows for more output power. With the polarization based output coupling scheme, adjusting polarization modes allows for control of polarization mode overlap and output coupling. When the pump and feedback polarization modes completely match, there is no output coupling. When there is complete output coupling, there is no oscillation due to high loss in the cavity. The output power can also be suppressed by simply adjusting one of the HWP.

A well behaved FOPO cannot be built by simply placing a highly nonlinear fiber inside a cavity. A spectral filtering, such as a prism or band pass filter is require to ensure singly resonant operation for less stringent requirements for phase matching.

Furthermore, the use of polarization optics gives more control over Fresnel reflections to reduce losses in the cavity.

In regards to designing a FOPO, using a PBS offers more flexibility for processes that require two tunable beams. Many groups reported using either a semi reflective end mirror, which has the drawback of polarization based losses, or a dichroic optic, which allows for output coupling of one field. Although [25] suggested output coupling the idler field while maintaining signal oscillation gives optimum FOPO operation, we suggest to output couple both signal and idler. By output coupling both fields we can three potential fields to work with for microscopy applications.

Conclusion

We observe that the input pump power must increase in order to increase output coupling, polarizing based output coupling allows for greater power, tunability, and flexibility of operation in comparison to a simple reflection approach at with the addition need to consider polarization states inside the FOPO cavity. Furthermore, attention to polarization states between the pump and feedback allows for one to obtain more average output power.

Table 3.9 gives a range of tunability of the system. The Raman wave number excitation is determined by:

$$\frac{1}{\lambda_p} - \frac{1}{\lambda_s} = \Omega \tag{3.2}$$

where λ_s and λ_p are the Stokes and pump field respectively in cm, and Ω is the Raman wavenumber in cm^{-1}.

From Table 3.9 we note that this system can cover a wide range of fingerprint wavenumber (1500 cm^{-1} and less). Although this FOPO has potential for applications in microscopy, the tuning range of this FOPO does not reach the desired 2800-3100 cm^{-1} for CH stretching imaging. Although there are other Raman modes to observe, CH stretching is the most commonly found in organic materials and specifically the most studied in terms of CRS signal measurement. Having the flexibility to observe both high frequency and fingerprint wavenumbers would be ideal. We planned to look for a signal at roughly 1400 cm^{-1} for C-H scissor, but the system had difficulty obtaining the required fields due to the method of tuning. The problem may be resolved by designing an automated tuning system. We decided to characterize another FOPO system with a tunable pump to offer more flexibility in probing different Raman regions.

Table of Tunability for Nd:Vanadate Laser

Pump (nm)	Stokes (nm)	Raman (cm^{-1})
960	1189	2006
971	1175	1788
968	1178	1842
976	1167	1677
980	1161	1591
991	1150	1395
995	1143	1301
987	1154	1466
960	1064	1018
971	1064	900
968	1064	932
976	1064	847
980	1064	806
991	1064	692
995	1064	652
987	1064	733
1064	1189	988
1064	1175	888
1064	1178	910
1064	1167	830
1064	1161	785
1064	1150	703
1064	1143	650
1064	1154	733

Table 3.10 Raman vibrational modes that can be obtained by the Nd:YVO_4 FOPO system. The colored boxes represent the mix between different fields: signal and idler (grey), signal and pump (blue), and pump and idler (yellow)

Chapter 4

Characterization of the Ti: Sapphire Pumped FOPO

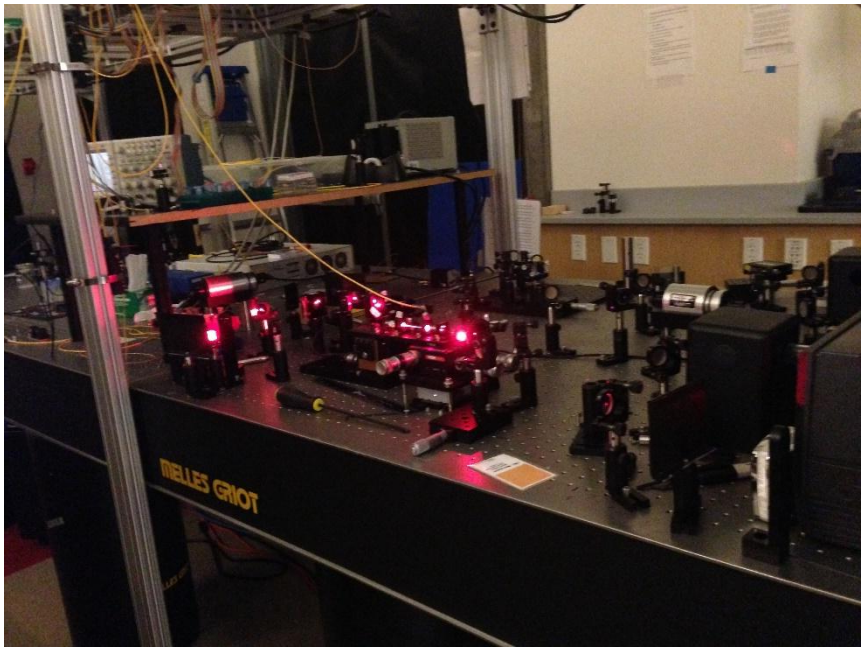

Figure 4.0 Image of oscillating Ti:Sapphire pumped FOPO

Introduction

Another system that we characterized is the Ti:Sapphire laser pumped FOPO. Although this system is not as compact as the system described in Chapter 3, using a Ti:Sapphire pumped system has many advantages. First, the ability to tune the pump to different wavelengths gives the flexibility in using different fibers to build the FOPO since fibers of different ZDW within the tunable range of 650 to 1100 nm can be used. Second, we can operate the FOPO in a state where noise can be minimized since we can tune the pump to obtain sidebands at the center of the FOPO tuning curve. This chapter compares the Ti:Sapphire FOPO to the Nd:YVO_4 FOPO and comments on other considerations important to performing CRS with a FOPO source.

System description of the Ti:Sapphire FOPO

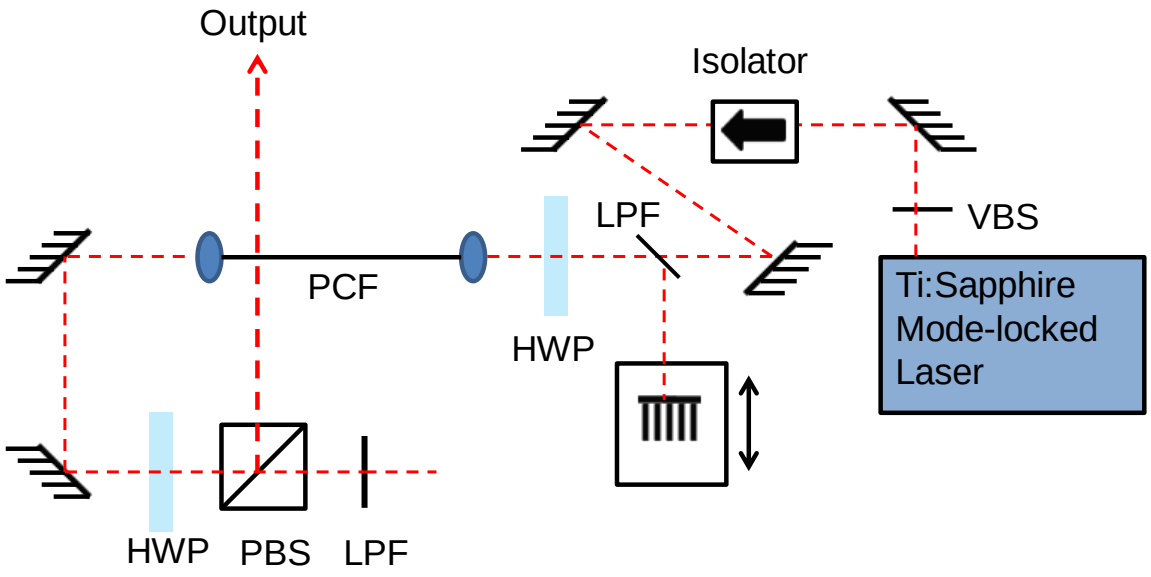

Figure 4.1 A schematic of the Ti:Sapphire FOPO system. The mirror on a translational stage and the reflection from the long pass filter (LPF) after the PBS form a Fabry-Perot cavity. The output coupling scheme is similar to the Nd:VO_4 FOPO system.

A schematic of the Ti:Sapphire laser pumped FOPO is given in Figure 4.1. The Ti:Sapphire laser emits 2 ps pulses at a repetition rate of 76.5 MHz. We set the center wavelength to be within 785 to 805 nm in order to maintain a working FOPO based on experimental observations. The VBS (Thorlabs NDC-50C-4M) at the output of the Ti:Sapphire laser controls the input power into the fiber. We use 4 cm polarization maintaining PCF with a core diameter of roughly 1 um with a ZDW near 820 nm. The input coupling lens is an aspheric lens (Thorlabs C230-TM-B) and the lens at the output of the fiber is an achromatic microscope objective (Olympus LMPlan IR). A HWP (Thorlabs AHWP05M-950) at the input end of the fiber optimizes the coupling into the fiber. At the output of the fiber, we utilize a polarization based output coupling scheme

that is similar to the set up described in Chapter 3. The mirror on translational stage and the 780 nm long pass filter (Chroma 780DCXXR) after the PBS (CVI Laser Optic, PBSH 450-1300-05) form a Fabry-Perot cavity. The LPF at the end of the cavity acts as the filtering mechanism to ensure singly resonant operation. There is roughly 2 m of free space in this system, which can be adjusted by the translation stage.

Large wavelength tuning can be done by tuning the pump, while fine wavelength tuning can be done through adjusting the cavity length of the end mirror or adjusting the angle of the end mirror and/or the LPF. Figure 4.2 gives a graph of the output wavelengths versus pump tuning and the corresponding phase matching diagram. The recorded spectra are for conditions with optimized output power (around 25 mW in both sidebands). As we tune the pump to longer wavelengths (closer to the ZDW), we observe that the wavelength spacing between signal and idler become closer to the pump.

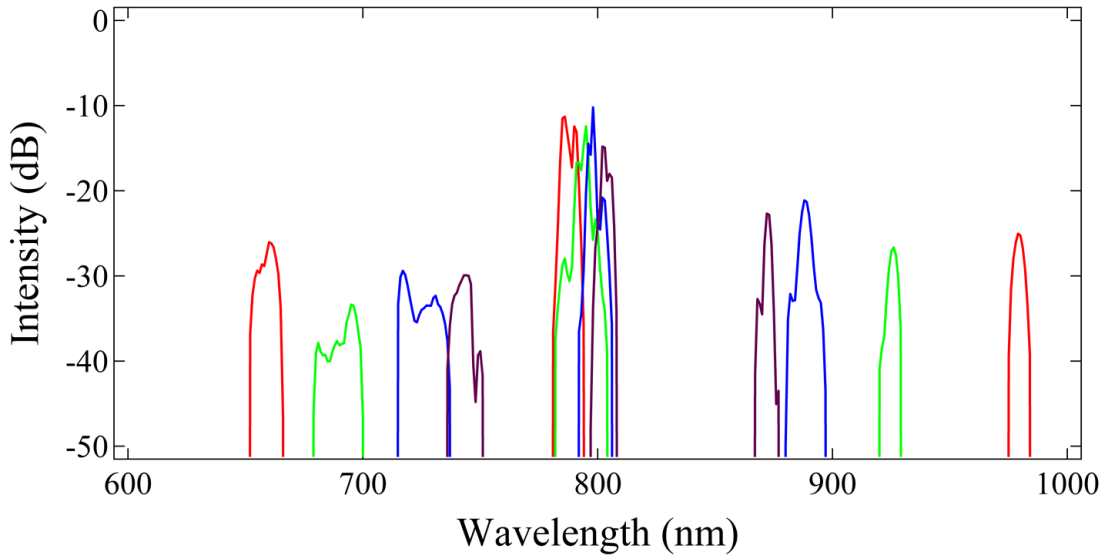

Figure 4.2 Tuning curve of the Ti:Sapphire pumped FOPO system. As we increase the pump wavelength to the frequency spacing between signal and idler become narrower.

Comparison to Nd:Vanadate FOPO

Table 4.3 summarizes the key comparisons between the two FOPO systems studied in this thesis. Both systems are similar in that both systems are mode-locked at high repetition rates (> 76 MHz) and emits picosecond pulses. Both systems have their advantages and disadvantages. We note some key points regarding the differences between the two systems.

Parameters	$Nd:YVO_4$	Ti:Sapphire
Input Wavelength	1064 nm	785-805 nm
Optimum total output power	140 mW	70 mW
Nonlinear Coefficient γ	10 $(W \cdot km)^{-1}$	40 $(W \cdot km)^{-1}$
Coupling Efficiency	0.67	0.35
Conversion Efficiency	0.26	0.20
Fiber Length	1.2 m	0.045 m
Fiber Core	5.0 um	1.4 um
Raman wavenumbers tunability (Signal and Idler)	1301 - 2006 cm^{-1}	1991 - 4937 cm^{-1}
Raman wavenumbers tunability (Signal and Pump)	651 - 1018 cm^{-1}	1006 - 2461 cm^{-1}
Raman wavenumbers tunability (Idler and Pump)	650 - 910 cm^{-1}	985 - 2476 cm^{-1}
Comments	High output power, low tunability, system is highly robust	Low output power, high tunability, fiber is susceptible to damage

Table 4.3 Comparison between the $Nd:YVO_4$ and Ti:Sapphire FOPO systems.

Complexity of the Pump Source

The pump sources for each system have different characteristics. The $Nd:YVO_4$ FOPO is a very stable system that is pumped by a passively mode-locked system. One can denote this system as a "turn-key" system because no additional adjustments are needed once the system is well aligned. However, the $Nd:YVO_4$ system only outputs 1064 nm light, which limits the tunability of the FOPO. However, one can tailor a fiber with the correct dispersion characteristics to generate the required frequencies commonly used for CRS microscopy.

In contrast, the Ti:Sapphire is not as stable as the $Nd:YVO_4$. The Ti:Sapphire is requires more attention to keep working. Temperature and humidity greatly affects the performance of the Ti:Sapphire laser. This system would not be a "turn-key" source that is desired for use in clinical settings. However, there are many advantages in using a Ti:Sapphire laser. First, the system can be tuned from 650 to 1100 nm with optimum operation at 800 nm. This allows for a wide range of tunability of the system can cover all the Raman modes of interest that are within 1000 cm^{-1} to 3500 cm^{-1}. Also, one can be lenient in terms of what fiber they use to build the FOPO because the wavelength of the laser can be shifted to match the ZDW of a fiber. Second, the Ti:Sapphire emits more output power than the $Nd:YVO_4$ system, which can translate to more output power from the FOPO. However, for this thesis the fiber used in the Ti:Sapphire system had less coupling efficiency. Third, Ti:Sapphire systems are commonly used in multiphoton microscopy systems. The fiber component of a FOPO enclosed in a box can allow for a Ti:Sapphire system to function as an OPO.

Operation

The difficulty in operation differs for both systems. The Nd:YVO_4 FOPO is difficult to align because the system the pump wavelength is in the near infrared (1064 nm). One must use an IR card or a IR scope for alignment. However, once the system has been well aligned the FOPO works as soon as the pump source is switched on. The optimization of output power however is complicated. Since the system uses a non-PM fiber we must utilize polarization optics such as half wave plates and fiber polarization controllers for optimizing output power. As noted in Chapter 3, one can obtain at least 20% more output power by adjusting the polarization optics from symmetric to asymmetric conditions.

In contrast, the difficulty in operating the Ti:Sapphire FOPO comes from the complexity of the pump source and the PCF. As stated earlier the Ti:Sapphire operation is dependent on temperature and humidity, and as a result can easily become un-mode-locked. The PCF used in this system has a smaller core diameter compared to the PCF used in the Nd:YVO_4 FOPO, which makes the system difficult to align. Aspheric lenses are used to focus light into the fiber. From experimental observations the output power of the Ti:Sapphire system can damage the front face of the fiber, affecting the coupling efficiency and FOPO operation. One would either need to cleave or replace the fiber in order to improve the coupling efficiency. Attenuating the input average pump power mediates the issue, but below 20% coupling efficiency (~200 mW) the system is at oscillation threshold. The pump wavelengths are within the visible range (785 to 800 nm), which makes alignment through the fiber easier to observe. The fiber used in this system is polarization maintaining, which resolves the issues with output coupling as found in the Nd:YVO_4 FOPO. Furthermore, the FOPO does not have complicated asymmetry versus symmetric conditions for output coupling due to the use of a PM fiber. We can simply adjust the HWP near the output coupler for optimum output power.

Tunability and Output Power

The Nd:YVO_4 FOPO can probe from 605 to 2006 cm^{-1} when looking at all the possible combinations of FOPO output. This does not reach the desired mode for imaging CH_2 stretching vibrational modes found from 2800-3100 cm^{-1}. However, one can probe CH_2 scissor at around 1500 cm^{-1} and amide I vibrations at around 1655 cm^{-1}, but the modes are not as strong as CH_2 stretching to be used for imaging [4]. Furthermore, in order to tune this system the FOPO is operated in a state where the oscillation is not optimum. We have performed experimental characterizations not covered in this thesis where the noise increases for the FOPO output as one detunes away from the optimum output power [29]. It is ideal to operate the FOPO in a regime where it is optimized for output power and low noise. A tunable laser would allow for one to optimize for output power for different output frequencies. In the case of this system the optimum output power (~70 mW) in each sideband occurs at 992 nm for signal and 1147 nm.

The Ti:Sapphire system has a much wider range of tunability, allowing for one to probe Raman modes from 985 to 4937 cm^{-1}. Fine tuning is similar to the Nd:YVO_4

system where the path length or angle of the feedback optics can be adjusted. With this system one can probe a wide range of modes with the potential of having low noise, since the FOPO output wavelengths can be tailored by adjusting the pump. However, due to the high nonlinearity of the PCF for this system, the power must be attenuated to generate narrow bandwidth output suitable for CRS microscopy. Figure 4.4 illustrates the power dependence on the bandwidth of the FOPO output.

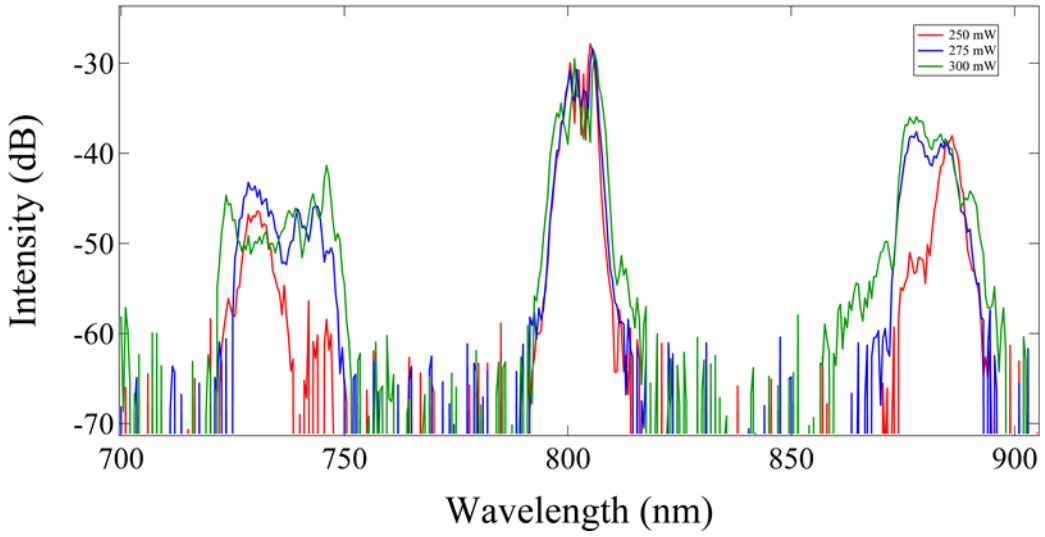

Figure 4.4 The dependence of power on the bandwidth of the sidebands for the Ti:Sapphire FOPO. As the input pump power increases, the sidebands generated become broader. This suggests that there is a trade-off between generating high average powers in the sidebands and having low spectral bandwidth.

Although the optimum observed output power is around 35 mW for in each sideband, the usable powers may be significantly less due to the spectral bandwidth of the sidebands which must be determined experimentally.

Selection of fields to utilize for CRS techniques

In general a FOPO system can output three frequencies (signal, idler, and pump), in which two different fields can be used for ω_s and ω_p in CRS techniques. By having a system that can output couple both signal and idler we have a system that is flexible in terms of probing a wide variety of Raman modes. For optimum resolution, one should utilize one sideband of the FOPO output and pump that is picked off from the input pump laser because the pump laser usually will have a narrowband output. It is not recommended to use the pump from the output of the FOPO because nonlinearity of the fiber broadens the pump bandwidth and decreasing the resolution of your signal. However, when presented with decent filters and a well behaved fiber, one can potentially generate narrowband FOPO output.

The disadvantage in utilizing the FOPO sideband output and pump is the difficulty in spatial and temporal alignment. In the case of the Ti:Sapphire FOPO, we attempted to build a delay line for pump so that the optical path length matches the FOPO

cavity, which required roughly 77 cm of extra free space. The free space might be resolved by coupling into a standard single mode fiber calculated to match the optical path length of the FOPO. It is difficult to confirm temporal overlap due to the difficulty in measuring ultrashort pulses with high resolution.

In using sideband and sideband for ω_s and ω_p, the temporal overlap is more relaxed because at the output FOPO system we can assume that the fields have a pretty close optical path length. We can utilize a Mach-Zender interferometer setup to adjust for the optical path length of the sideband output. Unless if the optimum PCF and filters are used, the output of the FOPO system may have a bandwidth that are wider than the Raman vibrations modes, which will affect the resolution of the CRS signal.

From Table 4.3 there are overlaps within the tuning ranges. For the Nd:YVO_4 system, pump with signal and idler with pump generates overlapping Raman wavenumbers from 650 to 910 cm^{-1}. For the Ti:Sapphire system signal with pump and idler with pump generates overlapping wavenumbers from 985 to 2461 cm^{-1}. For improving spatial resolution, one should utilize shorter wavelengths to generate the Raman vibration [4], and therefore signal and idler or signal and pump combinations would be ideal.

Components for CRS microscopy/spectroscopy

In tailoring a FOPO for CRS applications, there are many aspects to consider inside and outside the FOPO system. Within the FOPO cavity, one must consider the importance of selecting the correct lens for coupling into the fiber at both ends, having the correct focusing at the output coupler to improve tunability, and the appropriate filters for rejecting unwanted frequencies from the byproducts of nonlinear optics. In regards to operating the FOPO one must consider the input pump power's effect on the bandwidth of the generated sidebands. Outside of the FOPO cavity one must consider how to synchronize the designated pump and Stokes fields to achieve temporal and spatial overlap.

At the fiber input end, one would normally use an aspheric lens with high NA that matches the NA of the fiber to couple in as much light as possible into the core of the fiber. The drawback of using a high NA objective is the difficulty in alignment. Furthermore, if misaligned the tight focusing of the beam can potentially damage the front face of the fiber, which would affect the coupling efficiency. At the fiber output end, we have observed a decent amount of output power in using an aspheric lens with specifications that matched the aspheric lens at the input end. Due to the frequency dependence on the refractive index, the beam size of the side bands may not be the same size. This generates many issues. First, for generating a CRS signal the beam sizes should be similar in size so that there is optimum interaction between the designated pump and Stokes field. Second, since the beam sizes are different the temporal overlap incident at the sample may be affected. One way to bypass this issue is using an achromatic objective as the output coupler. Achromatic optics are ideal for CRS systems since the issue of chromatic dispersion can be circumvented.

Filters are important for allowing only the designated pump and Stokes field to interact with the sample. In highly nonlinear PCFs other $\chi^{(3)}$ processes such as third

harmonic generation can occur simultaneously with FWM, generating unwanted sidebands at much shorter wavelengths that are comparable in intensity to the output of the FOPO. We recommend using a long pass filter to filter out unwanted colors. The notch filter is another important component, which is tailored to filter out the pump, to allow for only the sideband and narrowband pump to interact with the sample. The notch filter of choice should have some bandwidth in filtering because the nonlinearity of the PCF broadens the pump and can cause leakage.

For most CRS techniques one would use linewidths that are close to the Raman excitation mode (1 nm) at FWHM. For the input pump power of our FOPO systems, we have observed that the bandwidth of the FOPO output generally increases with input pump power due to the intensity dependence in FWM. For the pump source, this is less of an issue because the pump output linewidth is generally narrow. For the FOPO output, due to the nonlinearity of PCFs the linewidth of sidebands generated can range from 5 nm up to 50 nm depending on input pump power. To mediate this issue of a broad linewidth for the sidebands one can use the pump for one field and using one of the sidebands as the other field and compensate the temporal overlap, which has been performed in CRS systems using broadband sources such as SC.

Conclusion

We have characterized two FOPO systems in regards to their tunability and output power for use in CRS microscopy. The Nd:YVO_4 FOPO offers high output power and is close to being a "turn-key" source due to the robustness of the system for CRS techniques, but there is the drawback cost of low tunability. The Ti:Sapphire FOPO offers a wide tunable range at the cost of having a more challenging mode of operation and lower output powers. Both systems can be potentially improved if the fiber used were tailored to their respective pump sources.

References

[1] C. W. Freudiger, W. Yang, G. R. Holtom, N. Peyghambarian, X. S. Xie, and K. Q. Kieu, “Stimulated Raman scattering microscopy with a robust fibre laser source”, Nat. Photon. 8, 153-159 (2014).

[2] Smith, Ewen, and Geoffrey Dent. *Modern Raman spectroscopy: a practical approach*. John Wiley & Sons, Chichester, U.K., (2005).

[3] S. Stewart, R. J. Priore, M. P. Nelson, and P. J. Treado, “Raman Imaging”, Annu. Rev. Anal. Chem., 5, 337-360 (2012).

[4] J. X. Cheng and X. S. Xie, *Coherent Raman Scattering Microscopy*, CRC Press, Florida, (2012)

[5] G. P. Agrawal, *Nonlinear Fiber Optics*, 4th ed., Academic Press, New York, (2006).

[6] C. L. Tang, W. R. Bosenberg, T. Ukachi, R. J. Lane, L. K. Cheng , "Optical parametric oscillators," *Proceedings of the IEEE* , vol.80, no.3, pp.365-374 (1992)

[7] H. Mojzisova and J. Vermot, "When multiphoton microscopy sees near infrared," Current Opinion in Genetics & Development, Volume 21, Issue 5, October 2011, Pages 549-557 (2011), 10.1016/j.gde.2011.08.004.

[8] C. W. Freudiger, W. Min, G. R. Holtom, B. Xu, M. Dantus, and X. S. Xie. “Highly specific label-free molecular imaging with spectrally tailored excitation-stimulated Raman scattering (STE-SRS) microscopy”, Nat. Photon. 5, 103-109 (2011)

[9] S. Lefrancois, D. Fu, G. R. Holtom, L. Kong, W. J. Wadsworth, P. Schneider, R. Herda, A. Zach, X. S. Xie, and F. W. Wise. "Fiber four-wave mixing source for coherent anti-Stokes Raman scattering microscopy." *Opt. Lett.* 37, (2012): 1652-1654 (2012).

[10] M. E. Marhic, *Fiber Optical Parametric Amplifiers, Oscillators and Related Devices* Cambridge Univ. Press, London, (2008)

[11] N. Dudovich and D. Oron. “Single-pulse coherently controlled nonlinear Raman spectroscopy and microscopy”, Nature 418, 512-514 (2003)

[12] H. Paulsen, K. Hilligse, J. Thøgersen, S. Keiding, and J. Larsen, "Coherent anti-Stokes Raman scattering microscopy with a photonic crystal fiber based light source”, Opt. Lett. **28**, 1123-1125 (2003).

[13] K. Wang, C. Freudiger, J. Lee, B. Saar, X. Xie, and C. Xu, "Synchronized time-lens source for coherent Raman scattering microscopy", Opt. Express **18**, 24019- 24024 (2010).

[14] Y. Zhai, C. Goulart, J. Sharping, H. Wei, S. Chen, W. Tong, M. Slipchenko, D. Zhang, and J. Cheng. "Multimodal coherent anti-Stokes Raman spectroscopic imaging with a fiber optical parametric oscillator" Appl. Phys. Lett. 98, 191106 (2011)

[15] S. Brustlein, P. Ferrand, N. Walther, et al; "Optical parametric oscillator-based light source for coherent raman scattering microscopy: practical overview", J. Biomed. Opt. 0001;16(2):021106-021106-10 (2010)

[16] H. T. Beier, G. D. Noojin, and B. A. Rockwell, "Stimulated Raman scattering using a single femtosecond oscillator with flexibility for imaging and spectral applications", Opt. Express **19**,18885–18892 (2011).

[17] E. S. Lamb, S. Lefrancois, M. Ji, W. J. Wadsworth, X. S. Xie, and F. W. Wise. "Fiber optical parametric oscillator for coherent anti-Stokes Raman scattering microscopy", Opt. Lett. 38, 4154-4157 (2013)

[18] E. Hecht, *Hecht Optics*. Addison Wesley, 997, 213-214, (1998)

[19] J. Hansryd, P. A. Andrekson, M. Westlund, J. Li, and P. Hedekvist, "Fiber-based optical parametric amplifiers and their applications," IEEE J. Sel. Top. Quantum Electron. 8, 506-520 (2002).

[20] C. Gu, C. Goulart, and J. E. Sharping, "Cross-phase-modulation-induced spectral effects in high-efficiency picosecond fiber optical parametric oscillators". Opt. Lett. 36, 1488-1490 (2011).

[21] Y. Xu, K. Mak, and S. Murdoch, "Multiwatt level output powers from a tunable fiber optical parametric oscillator," Opt. Lett. **36**, 1966-1968 (2011).

[22] L. Jin, A. Martinez, and S. Yamashita, "Optimization of output power in a fiber optical parametric oscillator," Opt. Express 21, 22617-22627 (2013).

[23] R. T. Murray, E. J. R. Kelleher, S. V. Popov, A. Mussot, A. Kudlinski, and J. R. Taylor, "Synchronously pumped photonic crystal fiber- based optical parametric oscillator," Opt. Lett.37, 3156–3158 (2012)

[24] C. Edward, *Field Guide to Polarization*. Vol. 15. Bellingham: SPIE Press, (2005).

[25] J. E. Sharping, "Microstructure Fiber Based Optical Parametric Oscillators", J. Lightw. Technol. 26, 2184, (2008).

[26] L. S. Kiani, T. Lu, and J. E. Sharping. "Comparison of Amplitude Noise of a Fiber Optical Parametric Oscillator and a Supercontinuum Source." *CLEO: Science and Innovations*. Optical Society of America, (2013)

[27] J. M. Dudley, and J. R. Taylor, "Ten years of nonlinear optics in photonic crystal fibre." *Nature Photonics, 3*(2), 85-90, (2009)